Phagosome resolution regenerates lysosomes and maintains the degradative capacity in phagocytes

Charlene Lancaster[1,2*], Aaron Fountain[3,4*], Elliott Somerville[3], Javal Sheth[1], Roaya M. Dayam[3,4,], Vanessa Jacobelli[3], Alex Somerville[3], Mauricio Terebiznik[1,2#] and Roberto J. Botelho[3,4#]

[1]Department of Biological Sciences, University of Toronto at Scarborough, Toronto, Ontario M1C 1A4, Canada, and [2]Department of Cell and Systems Biology, University of Toronto, Toronto, Ontario, M5S 3G5, Canada

[3]Department of Chemistry and Biology, [4]Graduate Program in Molecular Science, Ryerson University, Toronto, Ontario, Canada, M5B2K3

*These authors contributed equally to this work.

To whom correspondence should be sent to:

RJB at rbotelho@ryerson.ca

MT at mauricio.terebiznik@utoronto.ca

Running title: Phagosome resolution and lysosome regeneration

Keywords: Phagosomes, lysosomes, fission, organelles, macrophages, innate immunity, degradation, regeneration

Abbreviations: Arl 8: Arf-like GTPase 8**;** CLC-GFP: GFP-fusion of the clathrin-light chain**;** ConA: concanamycin A; DQ-BSA: dye-quenched bovine serum albumin; IKA: ikarugamycin**;** LAMP1: lysosomal-associated membrane protein 1**;** LAMP2: lysosomal-associated membrane protein 2; LB: Luria-Bertani medium**;** Lp**:** *Legionella pneumophila***;** mTORC1: mechanistic target of rapamycin complex 1; PDV: phagosome-derived vesicle**;** PtdIns(3)P: phosphatidylinositol 3-phosphate; PtdIns(3,5)P_2: phosphatidylinositol 3,5-biphosphate**;** PtdIns(4)P: phosphatidylinositol 4-phosphate**;** TFEB: transcription factor EB

Summary

Phagocytes engulf particles into phagolysosomes for degradation. However, the ultimate fate of phagolysosomes is undefined. Lancaster, Fountain et al. show that phagosomes undergo fragmentation to reform lysosomes in a clathrin-dependent manner. This process is necessary to maintain the degradative capacity of phagocytes during subsequent phagocytosis.

Abstract

During phagocytosis, phagocytes like macrophages engulf and sequester unwanted particles like bacteria into phagosomes. Phagosomes then fuse with lysosomes to mature into phagolysosomes, resulting in the degradation of the enclosed particle. Ultimately, phagosomes must be recycled to help recover membrane resources like lysosomes consumed during phagocytosis, a process referred to as phagosome resolution. Little is known about phagosome resolution, which may proceed through exocytosis or membrane fission. Here, we show that bacteria-containing phagolysosomes in macrophages undergo fragmentation through vesicle budding, tubulation, and constriction. Phagosome fragmentation required cargo degradation, the actin and microtubule

cytoskeletons, and clathrin. We provide evidence that lysosome reformation occurs during phagosome resolution since the majority of phagosome-derived vesicles displayed lysosomal properties. Importantly, we showed that the clathrin-dependent phagosome resolution is important to maintain the degradative capacity of macrophages challenged with two waves of phagocytosis. Overall, our work suggests that phagosome resolution contributes to lysosome recovery and to maintain the degradative power of macrophages to handle multiple waves of phagocytosis.

Introduction

Phagocytosis is the receptor-mediated engulfment of particulate matter, either of foreign origin, such as microbes and abiotic particles, or endogenous to the organism, such as apoptotic bodies, senescent cells, and transformed cells (Gray and Botelho, 2017; Levin et al., 2016; Henson, 2017; Lancaster et al., 2019). Hence, phagocytosis plays a critical role in infection resolution, tissue homeostasis and remodelling, and preempting cancer. Phagocytosis is initiated when cognate receptors expressed on phagocytes, such as macrophages, neutrophils, and dendritic cells engage ligands decorating the target particles (Gray and Botelho, 2017; Levin et al., 2016). This triggers a complex cascade of signals that are tightly coordinated in space and time to drive waves of actin assembly and disassembly and focal exocytosis of internal membrane stores to remodel the underlying plasma membrane, forming a phagocytic cup (Gray and Botelho, 2017; Levin et al., 2016; Niedergang and Grinstein, 2018). The phagocytic cup expands around a target particle, and eventually encapsulates the target particle within a phagosome (Gray and Botelho, 2017; Levin et al., 2016; Niedergang and Grinstein, 2018). Importantly, professional phagocytes like macrophages can engulf the equivalent of their entire surface area, indicating a significant exchange of internal and surface membrane pools (Cannon and Swanson, 1992; Aderem, 2002).

Phagosomes then undergo a maturation process characterized by the sequential conversion of an innocuous phagosome into a highly degradative and acidic phagolysosome, wherein particulates are digested (Gray and Botelho, 2017; Levin et al., 2016; Fairn and Grinstein, 2012; Pauwels et al., 2017). Phagosome maturation is stereotypically characterized by an early endosome-like stage, portrayed by the transient association of early endosome-associated factors like the Rab5 GTPases and the Vps34 Class III PI 3-kinase, which synthesizes phosphatidylinositol-3-phosphate [PtdIns(3)P] (Vieira et al., 2001; Fratti et al., 2001; Roberts et

al., 2000; Gutierrez, 2013). These early endosome determinants then recruit effectors like EEA1 and Hrs to phagosomes to mediate fusion with early endosomes and phagosome maturation (Fratti et al., 2001; Harrison et al., 2003; Vieira et al., 2003, 2004). However, on endosomes and at least on phagosomes enclosing apoptotic bodies, Rab5 then recruits the Mon1/Ccz1 complex to stimulate GTP-loading of the Rab7 GTPase (Kinchen and Ravichandran, 2010; Yasuda et al., 2016; Rink et al., 2005). Moreover, within 10 minutes of maturation, the phagosomal lumen acidifies to pH 6, causing the Vps34 complex to dissociate from early phagosomes (Naufer et al., 2018). This, combined with the conversion of PtdIns(3)P to phosphatidylinositol-3,5-bisphosphate [PtdIns(3,5)P_2] by PIKfyve, terminates PtdIns(3)P signaling (Kim et al., 2014; Hazeki et al., 2012; Naufer et al., 2018). In addition, phosphatidylinositol-4-phosphate [PtdIns(4)P] is also synthesized on late phagosomes and may mediate phagosome maturation as well (Levin et al., 2017; Jeschke and Haas, 2018). Collectively, the acquisition of Rab7, termination of PtdIns(3)P, and the synthesis of PtdIns(3,5)P_2 and PtdIns(4)P, all drive phagosome fusion with late endosomes and lysosomes, converting the early phagosome into a phagolysosome, which then possesses lysosomal determinants like the Arf-like GTPase 8 (Arl8), lysosomal membrane proteins like lysosomal-associated membrane proteins 1 and 2 (LAMP1 and LAMP2), a myriad collection of hydrolytic enzymes, and a luminal pH <5 established by the V-ATPase (Gray and Botelho, 2017; Levin et al., 2016; Kinchen and Ravichandran, 2010; Naufer et al., 2018; Kim et al., 2014; Garg et al., 2011; Levin-Konigsberg et al., 2019; Levin et al., 2017). This ensures digestion of particulates into its primordial components like amino acids and sugars, which are exported via transporters such as SLC-36.1 (at least in *Caenorhabditis elegans*) or by bulk via vesicular-tubular intermediates (Mantegazza et al., 2014; Gan et al., 2019).

The final stage of the life cycle of a phagosome is now referred to as phagosome resolution (Levin et al., 2016; Gray and Botelho, 2017). In unicellular eukaryotes like amoeba, phagosomes containing indigestible material are resolved via exocytosis, or egestion, expelling indigestible content and recycling the plasma membrane (Gotthardt et al., 2002; Stewart and Weisman, 1972). While this was assumed to occur in mammalian cells, recent work by the Overholtzer and Grinstein laboratories suggest that phagosomes undergo shrinkage and fission instead (Krajcovic et al., 2013; Krishna et al., 2016; Levin-Konigsberg et al., 2019). Partly, this occurs via the mechanistic target of rapamycin complex 1 (mTORC1) and PIKfyve-mediated mechanisms through unclear processes (Krajcovic et al., 2013; Krishna et al., 2016). In addition, PtdIns(4)P on phagolysosomes recruits SKIP/PLEKHM2 to secure kinesin motors to lysosomes via the Arl8b GTPase, which collectively drive membrane extrusion via phagosome tubules, aiding in phagosome resolution. Interestingly, ER-phagosome contact sites formed via Rab7 and the oxysterol-binding protein-related protein 1L (ORP1L) transfer phagosomal PtdIns(4)P to the ER for turnover and elimination of PtdIns(4)P from resolving phagolysosomes (Levin-Konigsberg et al., 2019).

Surprisingly, little else is known about phagosome resolution, including how phagosomal and endo-lysosomal membranes are recycled, or how phagocytes retune their endomembrane state after degradation of phagosomal contents. In particular, while phagocytosis activates the transcription factor EB (TFEB) to induce expression of lysosomal proteins, boosting lysosome and cytoprotective functions (Gray et al., 2016; Visvikis et al., 2014), phagosomes fuse with, and thus consume, “free” lysosomes during maturation, though we are not aware of a study that formally tested this. For long-lived phagocytes such as macrophages (van Furth and Cohn, 1968; Parihar et al., 2010), “free” lysosomes and other membranes must be replenished to allow these

cells to degrade multiple rounds of internalized particles over their lifetime. While evidence exists for plasma membrane resynthesis post-phagocytosis (Werb and Cohn, 1972), it is not actually known if and how lysosomes are reformed after phagosome maturation.

In this study, we report that phagosomes in macrophages undergo fission, tubulation, and splitting, culminating in phagosome fragmentation to reform lysosome-like organelles. We show that phagosome fragmentation required particle digestion, the actin and microtubule cytoskeleton systems, and clathrin. Moreover, we show that a first wave of phagocytosis reduced the number of "free" lysosomes and abated the degradative activity in phagosomes formed during a second round of phagocytosis. Importantly, "free" lysosomes were recovered, and the degradative power of secondary phagosomes was unabated in cells that were able to conduct clathrin-mediated phagosome resolution. Overall, our study reveals a role of phagolysosome resolution in the reformation of lysosomes for reuse by macrophages to sustain multiple rounds of phagocytosis.

Results

Phagolysosomes are not egested

Despite the extensive number of studies that have investigated phagocytosis and phagosomal maturation, very little is known about the terminal fate of the phagolysosome. For years, in textbooks, phagocytosis was assumed to end with the exocytosis of the phagolysosome. This idea of phagosomal secretion likely arose with the study of phagotrophic protozoans, which utilize exocytosis to remove indigestible material or waste from the cell (Clarke et al., 2002; Maniak, 2003; Stewart and Weisman, 1972; Gotthardt et al., 2002). However, more recent evidence suggests that mammalian phagosomes containing degradable cargo like apoptotic cells or red blood cells undergo shrinkage and/or fission (Krajcovic et al., 2013; Levin-Konigsberg et

al., 2019). To formally investigate if phagolysosomes containing indigestible material are secreted, we allowed RAW 264.7 murine macrophages to internalize IgG-opsonized latex beads and then followed the non-degradable cargo over 24-hours through live-cell imaging. Over this period, we did not observe neither exocytosis or release of phagosome-sequestered beads (Figure 1A and Video 1) and the number of beads per cell remained constant (Figure 1B). Treatment with the calcium ionophore, ionomycin, can induce lysosome exocytosis (Jans et al., 2004; Xu et al., 2013). Even with ionomycin treatment, beads were not expelled out of macrophages through exocytosis (Figure 1C and 1D, and Video 2). Altogether, these results indicate that phagosomes containing non-degradable beads are retained over long periods of time inside mammalian macrophages instead of undergoing exocytosis as is often assumed.

Phagolysosomes containing bacterial cargo undergo fragmentation

Recently, efferosomes and red blood cell-containing phagosomes were observed to undergo shrinkage and fragmentation (Krajcovic et al., 2013; Levin-Konigsberg et al., 2019). As these phagocytic targets are non-inflammatory, we thus queried whether phagosomes containing bacteria, which provoke an inflammatory response, would suffer a similar fate. We first utilized filamentous *Legionella pneumophila* (herein referred to as *Legionella* or Lp) expressing mCherry, which facilitates tracking during phagocytosis because of its size. The bacteria were paraformaldehyde (PFA)-killed before assays to avoid interference by its virulence effectors with the phagocytic pathway (Prashar and Terebiznik, 2015). As previously shown (Prashar et al., 2013), long filaments are internalized into phagosomes that coil around the nucleus and closely follows the shape of the encased bacteria. We then used live-cell imaging to track mCherry fluorescence as a proxy for the fate of bacterial cargo within phagosomes. We observed a

striking condensation of the bacterial cargo from intact filaments into spheroidal bodies within 7-20 h (Figure 2A and Video 3). The collapse of the filamentous phagosomes was accompanied by a gradual increase in cytoplasmic puncta labelled with mCherry that was originally expressed within *Legionella* (Figure 2A and Video 3). Ultimately, the original phagosomal compartment cannot be observed anymore, while a cloud of puncta remains (Figure 2A and Video 3). These observations indicate that bacteria-containing phagolysosomes undergo fragmentation, as the cargo degrades.

We further investigated this phenomenon by following mRFP1-*Escherichia coli (E. coli)*-containing phagosomes (Figure 2B, Video 4). This facilitated identification and quantification of phagosomes and phagosome-derived fragments because *E. coli* are quasi-homogenous in shape (rod) and size and mRFP1 is resistant to lysosomal degradation, permitting us to better track phagosome fragments (Katayama et al., 2008). Using Volocity, we were able to differentiate bacteria-containing phagosomes from puncta based on their fluorescence intensity and volume, which allowed us to calculate the total volume of phagosomes, as well as the total volume of phagosome-derived vesicles (PDVs) in each cell over time (more details about the quantification in Materials and Methods). As shown in Figure 2C, the total volume of phagosomes per macrophage decayed over time in a quadratic manner, while the total volume of PDVs increased exponentially over time, thus suggesting correspondence in the two phenomena. We further confirmed the observations from above through fixed-cell, population-based assays, where we found that the number of intact *E. coli* remaining within the macrophages decreased over time and corresponded with an increase in the number of puncta (Figure 2D and 2E).

While studying the dynamics of cargo fragmentation, we observed budding events that generated small vesicles both from early phagosomes and phagosome fragments (Figure 3,

Videos 5 and 6), tubulation events that either scissioned or collapsed back into the "mother" organelle (Figure 3, Video 7), or appeared to undergo constriction events to generate larger fragments rather than smaller vesicles (Figure 3, Video 7 and Video 8).

Finally, to further support the notion that phagosomes fragment even when they carry indigestible material, we prepared a semi-degradable cargo by aggregating fluorescently-labelled, 100 nm polystyrene nanobeads using IgG. We presumed that these bead clumps could be broken apart through IgG proteolysis within the degradative phagolysosome. Indeed, we observed that internalized bead clumps gradually formed a cloud of fluorescence or smaller puncta, suggesting that these phagosomes fission into smaller components (Supplemental Figure S1, Video 9). Thereby, these experiments reveal that phagolysosomes containing indigestible, yet modular particulate cargo, can also undergo fragmentation. Collectively, our data suggest that phagosome resolution proceeds through fragmentation, rather than exocytosis, and that multiple mechanisms of fragmentation are at play.

Phagolysosome fragmentation is dependent on cargo degradation and the cytoskeleton

Having observed that phagosomes containing bacteria undergo fragmentation via at least three morphologically-distinct processes (budding, splitting, and tubulation), we next set to understand some of the molecular players in phagosome resolution. First, we postulated that phagolysosome fragmentation required cargo degradation to facilitate membrane deformation and fission. To test this, we inhibited lysosomal proteases by exposing macrophages to a protease inhibitor cocktail or to NH_4Cl/ concanamycin A (Con A) mixture to alkalinize the lysosomal pH (Naufer et al., 2018; Li et al., 2013). First, vehicle-treated cells displayed a consistent increase in PDV volume 4 h after phagocytosis relative to 1 h post-phagocytosis, consistent with phagosome

fragmentation (Figure 4A-D). In comparison, cells treated with the protease cocktail or to NH_4Cl/ConA mixture displayed lower volume of PDVs 4 h after phagocytosis relative to the corresponding control cells (Figure 4A-D). Overall, these results indicate that cargo degradation is necessary for the fragmentation of the phagolysosome.

We then assessed the role of the cytoskeleton in phagosome fragmentation since the cytoskeleton is implicated in membrane scission driven by various mechanisms like coat protein assembly, motor-driven constriction, and membrane tubulation (Damiani, 2003; Gautreau et al., 2014; Ripoll et al., 2018; Bezanilla et al., 2015). For example, microtubules are necessary for the tubulation of autophagolysosomes, lysosomes, and phagolysosomes (Du et al., 2016; Harrison et al., 2003; Mrakovic et al., 2012; Vyas et al., 2007), whereas acto-myosin complexes are involved in the neck constriction and scission of phagosomes, as well as providing the mechanical force required to form membrane pits in endocytosis at mammalian synapses (Swanson et al., 1999; Wu et al., 2016). To assess the necessity of actin and microtubules in phagosomal fragmentation and the formation of PDVs, we allowed RAW macrophages to internalize mRFP1-*E. coli* for 40 min, before treatment with the actin and microtubule stabilizing drugs, jasplakinolide and taxol, respectively, as well as the actin and microtubule depolymerization drugs, cytochalasin D and nocodazole, respectively. Control cells showed extensive phagolysosomal fragmentation at 4 h post-phagocytosis relative to 1 h post-phagocytosis (Fig. 4E-H). In comparison, cells treated with either depolymerizing or stabilizing agents of microtubules and actin all displayed significantly lower PDV volume at 4 h post-phagocytosis relative to the corresponding control conditions (Figure 4E-H). Therefore, the actin and microtubule cytoskeletons are required for efficient fragmentation of the phagolysosome.

Clathrin is necessary for resolution of the phagolysosome

Clathrin is an important mediator of vesicle budding, which is well-known for its role at the plasma membrane during clathrin-mediated endocytosis and export from the trans-Golgi network (Kirchhausen et al., 2014). However, clathrin is also involved in budding events at the endosome, lysosome and autolysosomes (Stoorvogel et al., 1996; Traub et al., 1996; Rong et al., 2012). Given that budding events were observed to occur during phagosomal fragmentation, we investigated if clathrin is part of the machinery required to facilitate this process. We first observed clathrin dynamics during phagosome maturation and resolution using live-cell imaging of RAW macrophages expressing a GFP-fusion of the clathrin-light chain (CLC-GFP). Our observations revealed clusters of clathrin localized in close proximity to phagolysosomes containing beads or *Legionella* (Figure 5A, 5C). To better assess if clathrin was actually bound to phagosomes as opposed to coincidental co-localization, we isolated phagosomes and fixed these to help secure complexes to phagosomes before immuno-staining for LAMP1 and clathrin. In doing this, we observed clathrin-patches on isolated phagolysosomes, suggesting that clathrin is indeed physically associated with phagolysosomes (Figure 5B).

We then assessed the role of clathrin in phagosome fragmentation. We opted to do this by treating macrophages with two independent clathrin inhibitors, pitstop II and ikarugamycin, because we could control inhibition of clathrin after phagocytosis and formation of phagolysosomes; this avoided possible effects on phagocytosis and phagosome maturation that could compromise phagosome resolution. In addition, the use of these two independent drugs gives greater confidence that any observable perturbation of phagosome fragmentation is due to clathrin disruption. Using live-cell imaging of filamentous *Legionella*-containing phagosomes over 13 h post-phagocytosis, we observed that phagolysosomes within pitstop-treated cells did

not collapse to the same extent as in control cells, nor was there an increase in the volume of PDVs over many hours post-phagocytosis (Figure 6A, 6B and Video 10). Similarly, we observed a significant reduction in PDVs in pitstop and ikarugamycin-treated cells at 4 h post-phagocytosis using *E. coli* rods in fixed-macrophages, quantified by puncta volume (Figure 6C and 6D) and particle number (Figure 6E and 6F). Thus, using two inhibitors of clathrin and different approaches to track and quantify phagosome resolution, our data indicate that clathrin is necessary for phagosomal fragmentation.

Finally, the large GTPase dynamin is an essential component of the clathrin budding machinery, as it catalyzes the scission of clathrin-coated vesicles from the plasma membrane and other organelle membranes (Mettlen et al., 2009). To assess if dynamin is also involved in the resolution of phagosomes, we utilized the pharmacological inhibitor dyngo-4a, which inhibits dynamin. As observed for clathrin inhibitors, dyngo-4a-treated cells produced a significantly smaller total volume of PDVs than in control cells 4 h post-phagocytosis (Supplemental Figure S2A-S2B). Collectively, these results indicate that the resolution of the phagolysosome is at least in part mediated by clathrin machinery.

Phagosome-derived vesicles have lysosomal characteristics

Our results indicate that the phagolysosome is fragmented into punctate-like membrane compartments in macrophages and that this likely involves multiple mechanisms. To investigate if the phagosomal fragments retained a predominant lysosomal character, we looked at their association with endo-lysosomal markers. First, macrophages were challenged with ZsGreen-*E. coli*, followed by 6 h chase to elicit phagosome fragmentation, then fixed and immunostained against for the lysosomal-associated membrane protein 1 (LAMP1) and LAMP2. As shown in

Figure 7A and 7B, approximately 80% of PDVs (defined as ZsGreen-positive compartments with an area >0.1 μm^2 but <4 μm^2 to exclude the parental phagosomes) were positive for LAMP1 and LAMP2 (Figure 7A and 7B). We next determined if PDVs were acidic and proteolytically-active. For these purposes, we respectively utilized LysoTracker Red, a membrane-permeable and acidotrophic fluorophore, and the Magic Red Cathepsin L substrate, which produces fluorescence once cleaved by cathepsin L. We observed that > 80% of PDVs were acidic and proteolytically-active with little change between 6 h and 20 h post-phagocytosis (Figure 7C-7F). Altogether, our findings reveal that phagolysosome-derived compartments retain endo-lysosomal features of the mother phagolysosome.

Phagolysosome fragmentation reforms lysosomes

During phagosome maturation, phagosomes extensively fuse with lysosomes, which presumably consumes and reduces "free" lysosomes, potentially exhausting the degradative capacity of the phagocyte. Given that macrophages are long-lived and can undertake multiple successive rounds of phagocytosis (Cannon and Swanson, 1992; Parihar et al., 2010; van Furth and Cohn, 1968), we postulated that phagosome fragmentation may participate in lysosome reformation and maintaining the degradative capacity of macrophages.

To test this hypothesis, we first assessed the number of LAMP1-positive puncta as a proxy for "free" lysosomes in resting macrophages or after phagocytosis of indigestible latex beads, precluding phagosome resolution. Indeed, there were significantly fewer "free" lysosomes in macrophages that engulfed latex beads and undertook phagosome maturation (60 min) relative to resting macrophages or those that undertook phagocytosis but had limited time to fuse with lysosomes (15 min; Figure 8A and 8B). In comparison, there was no significant difference in

"free" lysosome number between resting macrophages and those undertaking early phagosome maturation, consistent with low phagosome-lysosome fusion and demonstrating that our quantification method was not affected by bead crowding in the cytoplasm (Figure 8A and 8B).

To help determine if phagosome resolution aids in lysosome regeneration, we then employed degradable *Legionella* filaments; these form extensive phagosomes that tend not to overcrowd the cytoplasm because of coiling, thus further facilitating visualization of lysosome number. Free lysosomes were quantified by applying a mask on fluorescent *Legionella* filament and quantifying the number of LAMP1-positive puncta outside of this mask. We compared resting cells, cells with *Legionella*-containing phagosomes for 2 h or 6 h post-phagocytosis to respectively elicit phagosome-lysosome fusion (2 h) and fragmentation (6 h). As with the latex bead-containing phagosomes, cells that were incubated for 2 h post-phagocytosis suffered a 45% reduction in the number of "free" lysosomes (Figure 8C and 8D). Interestingly, and relative to 2 h post-phagocytosis, we observed a significant increase in the number of "free" lysosomes after the onset of phagosomal fission (6 h; Figure 8C and 8D), suggesting that macrophages began to recover LAMP1-positive lysosomes through phagosomal fragmentation.

We next hypothesized that phagosome-derived lysosome-like compartments can fuse with subsequent phagosomes. To test this, we challenged macrophages with two rounds of phagocytosis. In one model, we allowed macrophages to engulf PFA-killed mCherry-expressing *Legionella* followed by a 6 h chase to prompt phagosome resolution. We then challenged these macrophages to engulf latex beads followed by 1 h of phagosome maturation. We observed transfer of mCherry that originated from within *Legionella* (first phagocytosis) onto bead-containing phagosomes (second phagocytosis; Figure 9A and 9B). In a second model, macrophages were allowed to form phagosomes containing mRFP1-*E. coli* (first phagocytosis)

for 1 h, followed by no chase period (0 h) or 2 h to begin phagosome resolution. Macrophages were then challenged with ZsGreen-expressing *E. coli* as the second wave of phagocytosis and chased for 1 h to elicit maturation. Using this model, macrophages that were given time to resolve the first phagosomes exhibited a higher degree of mRFP1 colocalization with secondary phagosomes enclosing ZsGreen-*E. coli* than macrophages deprived of a chase time period (Figure 9C and 9D). Altogether, these observations suggest that PDVs fuse with secondary phagosomes, consistent with these being lysosome-like organelles.

Clathrin-mediated phagosome fragmentation is required to recover degradative capacity

Given that lysosomes are consumed through phagolysosome formation, we surmised that this may reduce the degradative capacity of macrophages. In turn, secondary phagosomes may exhibit lower degradative activity. To test this hypothesis, we again employed a primary wave of phagocytosis using either IgG-opsonized latex beads or *E. coli*, followed by a second phagocytic wave using IgG-opsonized beads and coated with the dye-quenched bovine serum albumin (DQ-BSA), which become increasingly fluorescent with augmented proteolytic activity. Indeed, we observed that the fluorescence of DQ-BSA-coated beads was decreased in macrophages that internalized a primary target of beads or *E. coli* 1 h earlier compared to macrophages with no prior phagocytosis (Figure 10A and 10B, blue bars in mock primary vs. blue bars in 1 h *E. coli* or 1h beads). Importantly, the proteolytic activity of secondary phagosomes recovered significantly in macrophages chased for 6 h after engulfing *E. coli* (Figure 10A and 10B; blue vs. red bars in *E. coli* condition). Conversely, there was no difference in DQ-BSA-bead fluorescence at 1 h or 6 h post-uptake of indigestible primary beads (Figure

10A and 10B, blue vs. red bars in primary bead condition). Collectively, these observations indicate that the degradative capacity of macrophages decreases with phagocytosis but is recovered through phagosomal resolution.

We then aimed to test whether clathrin-mediated phagosome resolution was required for macrophages to regain their degradative capacity. To do these experiments, we had to expose macrophages for 6 h to vehicle or ikarugamycin post-phagocytosis to elicit phagosome resolution. This prolonged clathrin inhibition raised concerns because of potential detrimental effects to basal macrophage function. To account for this, we assessed the degradative activity of phagosomes containing DQ-BSA-beads in macrophages without prior phagocytosis (no primary) and that were exposed to vehicle for 1 h or 6 h, or to ikarugamycin for 6 h. Indeed, we observed a significant drop in the proteolytic activity associated with phagosomes sequestering DQ-BSA-beads in cells treated with ikarugamycin relative to those exposed to vehicle for 1 h or 6 h (Figure 10C and 10D). This perturbation in phagosome-associated proteolytic activity likely represents an impairment in biosynthetic trafficking of proteases.

We then examined the combined effect of clathrin inhibition and prior phagocytosis. First, macrophages that engulfed *E. coli* 1 h prior had significantly lower DQ-BSA fluorescence in secondary phagosomes than those macrophages without primary phagocytosis (Figure 10C and 10D, blue dots in mock phagocytosis vs. *E. coli* phagocytosis), consistent with consumption of lysosomes by the first wave of phagosomes. Second, there was a significant increase in DQ-BSA fluorescence in macrophages that engulfed *E. coli* 6 h prior relative to those had engulfed *E. coli* 1 h prior (Figure 10C and 10D, blue and red dots under *E. coli* primary phagocytosis). This is consistent with results in Figure 10A-B. Importantly, this recovery was abolished when cells were pre-treated with ikarugamycin for 6 h (Figure 10B and 10C, green dots vs. blue and

red dots under E. coli primary phagocytosis). We then ascertained if the combined effect of clathrin inhibition and phagocytosis was greater than clathrin inhibition alone. This was done by normalizing the fluorescence of DQ-BSA-bead from ikarugamycin-treated cells to vehicle-treated cells in cells with one round versus two-rounds of engulfment. Our data show a significant abatement in this ratio for macrophages that undertook two rounds of phagocytosis relative to those that engulfed only DQ-BSA-beads (Figure 10E). Collectively, these data suggest that hindering clathrin profoundly impairs proteolytic recovery after phagocytosis.

Discussion

For every phagosome formed, membrane resources, including plasma membrane, endosomes, and lysosomes, are consumed and thus membrane resynthesis or retrieval is critical for the continuing functioning of the phagocyte (Zent and Elliott, 2017). However, it is largely uncharacterized how phagocytes recover cellular resources, though synthesis of plasma membrane lipids has been observed (Werb and Cohn, 1972). Here, we show that macrophages resolve phagosomes through fragmentation of the compartment and not through exocytosis. This fission process is dependent on the degradation of the cargo, the cytoskeleton, clathrin and dynamin. Moreover, we present evidence that phagolysosome resolution is critical in reforming lysosomes that have been consumed during phagosome maturation and is important for the maintenance of proteolytic activity within macrophages that continuously undergo phagocytosis.

The ultimate fate of phagolysosomes

For years, it was generally assumed that phagolysosomes underwent exocytosis to expel indigestible material and return membrane to the surface of the phagocyte. This paradigm was based on observations made with protozoans (Stewart and Weisman, 1972; Maniak, 2003; Clarke et al., 2002; Gotthardt et al., 2002). However, secreting phagosomal remnants onto multicellular tissues is potentially detrimental to tissue homeostasis. Indeed, we failed to collect evidence supporting phagosome exocytosis containing bacteria or indigestible beads. Instead, we observed an accumulation of smaller, membrane-bound compartments within the cytoplasm of macrophages that were derived from phagosomes, as well as the disappearance of recognizable phagosomes. This phagosome fragmentation proceeded through phagosomal splitting, tubulation, and budding, suggesting at least three distinct mechanisms that we discuss below. Recently, independent work by the Overholtzer and Grinstein groups respectively tracked efferosomes and phagosomes containing red blood cells and observed that both shrunk or fragmented into phagosome-derived membrane compartments, as well (Krajcovic et al., 2013; Levin-Konigsberg et al., 2019). Collectively, all these observations suggest that phagosome resolution is commonly realized by phagosome fragmentation through distinct mechanisms of membrane fission rather than exocytosis, irrespective of whether the cargo is host-derived, bacterial, or even abiotic. Yet, we emphasize that we have not excluded exocytosis as a mechanism of phagosome resolution for all modes of phagocytosis, such as the uptake of naturally occurring indigestible respirable particulates captured by alveolar macrophages or resolution of phagosomes with pathogenic microorganisms; indeed, phagosomes containing *Cryptococcus neoformans* were observed to undergo expulsion (Ma et al., 2006; Alvarez and Casadevall, 2006). This will need to be further explored.

In addition, while tubulation, budding, and splitting are detectable during phagosome resolution, it is important to state that membrane fission occurs throughout the lifecycle of the phagosome, not simply during resolution (Saffi and Botelho, 2019). For example, COPI-mediated fission occurs on phagosomes to extract transferrin receptor from early phagosomes (Botelho et al., 2000), while cytoskeleton mediates recycling from phagosomes enclosing non-digestible latex beads (Damiani, 2003). Moreover, MHC-II::peptide complexes exit phagosomes likely before resolution ensues, though the exact mechanism and timing is unclear (Harding and Geuze, 1992; Mantegazza et al., 2013, 2014; Ramachandra et al., 1999). Finally, tubules can dynamically form between phagosomes to exchange phagosomal content with implications towards antigen presentation (Mantegazza et al., 2014). All these processes occur before phagosomes become unidentifiable as such. Thus, we propose a model in which membrane fission happens throughout the life-cycle of the phagosome, where early and mid-maturation serves to sort and remove cargo from the phagosome without leading to disintegration of the phagosome, whereas end-of-life fission culminates in phagosome disappearance. Whether the fission processes that act throughout the life-cycle of the phagosome are distinct or similar but subject to divergent regulatory inputs remains unknown, but we argue that this is an exciting and poorly defined aspect of phagosome maturation.

Cargo degradation in phagolysosome resolution

Through inhibition of lysosomal proteases and neutralization of the phagosomal pH, we provide evidence that cargo degradation is required for phagosomal resolution. Mechanistically, we envision two non-mutually exclusive possibilities for this requirement. First, cargo degradation may be a physical requirement for phagosome fission. Supporting this concept, large latex beads

remain enclosed within phagosomes for prolonged periods of time likely because of physical restriction. On the other hand, nanobead clusters can fragment through degradation and disaggregation of IgG. Second, digestible cargo like bacteria, contains a complex mix of macromolecules that are degraded to release monomers like amino acids that become available for use within the phagocyte. This bolus of amino acids may be sensed by intraluminal amino acid sensors like the V-ATPase or by cytoplasmic sensors like CASTOR after amino acid transport across the phagolysosome membrane, locally promoting mTORC1 activation (Saxton et al., 2016; Chantranupong et al., 2016; Zoncu et al., 2011; Inpanathan and Botelho, 2019). While mTORC1 drives many anabolic processes like protein and lipid synthesis, mTORC1 also plays a role in coordinating phagosome and lysosome dynamics, including efferosome fission (Krajcovic et al., 2013; Inpanathan and Botelho, 2019; Saric et al., 2016; Hipolito et al., 2019). Thus, cargo degradation coupled to mTORC1 activation could help orchestrate phagosome resolution. This would parallel the role of mTORC1 re-activation during degradation of autophagic cargo to regenerate lysosomes (Yu et al., 2010).

Requirements for phagosome resolution

In addition to cargo degradation, we observed that drugs that stabilized or depolymerized the actin and microtubule cytoskeletons, and inhibitors of clathrin and dynamin, all impaired phagosome fragmentation. Together with our observations that phagosomes suffer splitting, tubulation, and budding, this implies that multiple mechanisms are at play during phagosome resolution. Potentially, actin may play a role in membrane constriction through assembly of acto-myosin complexes to help distort phagosomes (Liebl and Griffiths, 2009; Curchoe and Manor,

2017). Alternatively, short branched actin assemblies are associated with fission of endosome/lysosomes through contacts with the endoplasmic reticulum (Rowland et al., 2014; Hoyer et al., 2018). For example, the actin-nucleating protein Wiskott–Aldrich syndrome protein and SCAR homologue (WASH) and FAM21 are recruited to sites of membrane tubulation and fission at ER-endosome contact sites (Dong et al., 2016; Rowland et al., 2014; Hoyer et al., 2018). Interestingly, ER-phagosome contact sites emerged recently as mediators of phagosome tubulation wherein lipid exchange was mediated by local pools of PtdIns(4)P (Levin-Konigsberg et al., 2019). This could also be coupled to microtubule dynamics since microtubules play a prominent role in membrane extrusion through tubulation under different contexts, which include LPS-mediated lysosome tubulation in phagocytes, early phagosome tubulation, tubulation during autophagic lysosome reformation, and endosome tubulation (Du et al., 2016; Delevoye et al., 2014; Mrakovic et al., 2012; Vyas et al., 2007; Harrison et al., 2003). This likely depends on the combined action of dynein and kinesin motor proteins modulated by Rab7 and/or Arl8b GTPases (Jordens et al., 2001; Garg et al., 2011). However, a challenge in assessing the role of these proteins in phagosome resolution is that they are also required for maturation; thus, disturbing the function of proteins like Rab7 and associated effectors would preclude phagosome resolution by interfering with maturation (Harrison et al., 2003; Garg et al., 2011). The development of tools that can deactivate these proteins acutely is necessary to dissect their roles in phagosome maturation versus resolution.

Finally, using independent compounds like ikarugamycin, pitstop, and dyngo-4a, we found that clathrin and dynamin play an important role in budding events at the phagolysosome. The role of clathrin on lysosomes remains poorly defined, despite early observations in the 1990s that clathrin associates with lysosomes and that multiple adaptor protein complexes act on

lysosomes or lysosome-like organelles (Arneson et al., 1999; Traub et al., 1996; Saffi and Botelho, 2019). More recently, clathrin and adaptor protein complexes like AP-2 were discovered to have a critical role in lysosome regeneration from spent autolysosomes. Specifically, distinct PIPKI isoforms are recruited to spent autolysosomes to locally generate two sequential bursts of PtdIns(4,5)P_2. The first burst leads to assembly of clathrin to nucleate a tubule, followed by a second burst of PtdIns(4,5)P_2 at the tips of the tubules that helps induce clathrin-mediated vesiculation of lysosome precursors (Rong et al., 2012). Whether a similar process occurs on resolving phagosomes is unknown, though we note that autophagic lysosome reformation is likely a collection of distinct processes since other tubules were observed to form from autolysosomes in a manner depending on PtdIns(3)P and PtdIns(4)P (Sridhar et al., 2013; Munson et al., 2015; Saffi and Botelho, 2019).

Lysosome consumption and regeneration during phagosome resolution

We provide evidence that phagocytosis and phagosome maturation consume “free” lysosomes and consequently abate the degradative capacity of subsequently formed phagosomes. However, we also observed that this is a transient phenomenon since over time, cells that contained phagosomes with degradable cargo more rapidly: i) recovered the number of free lysosomes and ii) subsequently formed phagosomes displaying higher proteolytic activity compared to cells that had yet to undergo phagosome resolution or engulfed indigestible cargo. Importantly, clathrin inhibition impaired phagosome resolution and prevented secondary phagosomes from acquiring higher degradative activity. Admittedly, prolonged clathrin inhibition is a complex manipulation likely to have indirect effects. Indeed, clathrin inhibitors alone caused a reduction in the

degradative capacity of phagosomes, likely by impairing trafficking of newly synthesized hydrolases (Borgne and Hoflack, 1997; Ludwig et al., 1994). Nevertheless, the combined effect of clathrin inhibition and phagosomal load synergistically hindered the proteolytic activity of secondary phagosomes. This suggests that failure to undergo resolution of earlier phagosomes pre-empted lysosome regeneration and reduced macrophage capacity to deal with subsequent phagocytosis.

Overall, we propose that phagosome resolution helps regenerate lysosomes consumed during phagosome maturation. This is consistent with 80% of phagosome-derived fragments displaying lysosome properties including possessing lysosomal proteins, displaying acidic and proteolytic activity, and fusogenicity towards new phagosomes. However, we suspect that phagosome-derived vesicles are heterogeneous and may represent distinct endo-lysosome intermediates. This may include fully functional lysosomes or proto-lysosomes that are depleted of degradative capacity as observed during autophagic lysosome reformation (Yu et al., 2010). Interestingly, we previously showed that phagocytosis activates TFEB to induce lysosome gene expression and boost lysosome function and bactericidal activity (Gray et al., 2016). Conceivably, TFEB activation may also be coupled to lysosome regeneration during phagosome resolution to recharge regenerated lysosomes.

Materials and Methods

Cell culture, transfection and mammalian expression constructs

RAW 264.7 murine macrophages (ATCC TIB-71™, American Type Culture Collection, Manassas, VA, USA) were cultured at 37°C and 5% CO_2 in DMEM supplemented with 10%

heat-inactivated FBS (Wisent Inc., St-Bruno, QC, Canada). Macrophages were transfected using FuGENE HD (Promega Corp., Madison, WI, USA) based to the manufacturer's instructions and were utilized following overnight expression of the construct. The clathrin light chain-GFP construct was a gift from Dr. Costin Antonescu and previously described in (Aguet et al., 2013).

Preparation of bacterial targets

To obtain fluorescently-labelled *E. coli*, the DH5α *E. coli* strain was transformed with the pBAD::mRFP1 plasmid (Addgene plasmid #54667; Campbell et al., 2002) or the pZsGreen vector (cat. # 632446; Takara Bio USA, Inc., Mountain View, CA, USA). Transformed *E. coli* were grown overnight at 37°C on Luria-Bertani (LB) agar plates and colonies were subsequently cultured overnight at 37°C in LB broth under agitation, where both plates and broth were supplemented with 100 µg/mL ampicillin (Bioshop Canada Inc., Burlington, ON, Canada. For ZsGreen-*E. coli*, 1% D-glucose (Bioshop Canada Inc.) was also added to the LB plates and broth to suppress leaky expression of ZsGreen from the *lac* operon. The overnight cultures were subcultured at 1:100 dilution and grown at 37°C until mid-log phase, at which time mRFP1 expression was induced through supplementation with 5 mM L-arabinose (Bioshop Canada Inc.) for 4 h, while ZsGreen expression was induced with 1 mM IPTG (Sigma Aldrich, Oakville, ON, Canada) for 3 h. The *E. coli* cultures were subsequently fixed in 4% paraformaldehyde (PFA; Electron Microscopy Sciences, Hatfield, PA, USA) in phosphate-buffered saline (PBS).

To obtain fluorescently-labelled filamentous targets, mCherry-*L. pneumophila* were prepared as described (Prashar et al., 2013). Briefly, *L. pneumophila* containing the KB288 plasmid, a gift from Dr. A.K. Brassinga and described in (Brassinga et al., 2010), were first grown at 37°C and 5% CO_2 on buffered charcoal-yeast extract plates for 3 days. Colonies were

grown for an additional 24 h at 37°C in buffered yeast extract (BYE) media under agitation. The *Legionella* filaments were then killed with 4% PFA solution. For the analysis of phagosome resolution utilizing filaments, bacteria longer than 15 µm were considered filamentous (Prashar et al., 2013).

Phagocytosis assays

For the phagocytosis of *Legionella* filaments, the bacteria were opsonized with 0.1 mg/mL of anti-*Legionella* antibody (Public Health Ontario, Toronto, ON, Canada) for 1 h at room temperature (RT; Prashar et al., 2013). RAW macrophages were pre-cooled to 15°C for 5 minutes before the cells were challenged with filaments at a ratio of 150 filaments per macrophage. Bacterial attachment was synchronized by spinning the cells at 300 x g for 5 minutes at 15°C. Following a 15-minute incubation at 37°C, unbound filaments were washed off with PBS. Macrophages were subsequently incubated at 37°C to allow phagocytosis to progress to the indicated time points, at which time the cells were either fixed with 4% PFA for 20 minutes or imaged live.

For the phagocytosis of *E. coli* rods and beads, the bacteria, 3.87 µm polystyrene latex beads (Bangs Laboratories, Fishers, IN, USA) or 3.0 µm polystyrene latex beads (Sigma Aldrich) were opsonized with 4 mg/mL of human IgG (Sigma Aldrich) for 1 h at RT. To coat beads with DQ-BSA, a 5% w/v solution of 3.0 µm beads was opsonized with 0.5 mg/mL DQ-Red BSA (ThermoFisher Scientific, Mississauga, ON, Canada) for 1 h before human IgG opsonization. RAW cells were pre-cooled to 4°C for 5 min prior to the cells being presented with targets at ratios of 20-400 rods per cell, 10 3.87 µm beads per cell or 25-135 3.0 µm beads per cell, depending on if phagosomal saturation was required. Target attachment was synchronized

by spinning cells at 300 x g for 5 min at 4°C. Following a 15- to 60-minute incubation at 37°C, unbound targets were washed off with PBS. The cells were then incubated at 37°C to allow phagocytosis to progress to the indicated time points and either fixed with PFA or imaged live. For assays using two-rounds of phagocytosis, the procedure for both the first and second rounds of phagocytosis was the same as described above, except the secondary phagocytic challenge was done after the first round of phagocytosis at specified times. The secondary challenge was then followed with no chase or 1 h chase to elicit further maturation, prior to fixation or live cell imaging.

For the phagocytosis of bead clumps, 0.1 µm Tetraspeck microspheres (blue/green/orange/dark red; Thermo Fisher Scientific) were opsonized with 4 mg/mL of human IgG for 1 hour at RT before leaving the mixture at 4°C overnight. Macrophages were pre-cooled to 4°C for 5 min prior to the cells being presented with bead clumps at ratios of 1,400 beads per cell. Bead clumps were spun onto the cells at 300 x g for 5 min at 4°C. Following a 15-minute incubation at 37°C, unbound bead clumps were washed off with PBS. Macrophages were subsequently incubated at 37°C to allow phagocytosis to progress to the indicated time points, at which point the cells were imaged live.

Isolation of phagosomes

To isolate phagosomes, a sucrose gradient was prepared by adding 1 mL of 60% sucrose suspension to a 1 mL ultracentrifuge tube and the solution was centrifuged at 50,000 xg for 1 h at 4°C. Following centrifugation, the sucrose gradient was carefully placed on ice until ready to use. Macrophages were allowed to internalize IgG-opsonized polystyrene beads for 60 min. Following phagocytosis, the cell media was replaced with cold homogenization buffer (20 mM

Tris (Bioshop), 1:400 protease inhibitor cocktail (Sigma), 1 mM AEBSF (Bioshop), 1 mM $MgCl_2$ (Thermo Scientific), 1 mM $CaCl_2$ (Biobasic, Markham, ON, Canada), 0.02 mg/mL RNase (Roche Diagnostics, Laval, QC, Canada), and 0.02 mg/mL DNase (Roche), pH 7.4), and the cells were dislodged by mechanical scraping. The cell suspension was centrifuged at 500 xg for 5 minutes at 4°C, and the pellet was resuspended in homogenization buffer. Cells were lysed by passing the suspension through a 22-gauge needle 5-10 times, then the lysate was centrifuged at 1000 xg for 5 min. The pellet was resuspended in 4% PFA and incubated at room temperature for 20 min to fix the lysate and secure protein complexes on the phagosome surface. The pellet was washed 3 times with PBS followed by centrifugation at 3000 xg for 5 min per wash, then resuspended in 200 µL of PBS. To separate phagosomes from the resuspended lysate pellet, the resuspended pellet was loaded onto the sucrose gradient and then centrifuged at 21,000 xg for 10 min at 4°C. The bead-containing fraction was extracted from the gradient with a 22-gauge needle and washed with ice-cold PBS.

Pharmacological inhibitors

Inhibitors and the DMSO (Bioshop) vehicle control were applied post-phagocytosis and maintained until fixation or the conclusion of the experiment. To increase cytosolic Ca^{2+}, cells were incubated with 10 µM of ionomycin (Sigma-Aldrich) and 1.2 mM of $CaCl_2$ (Bioshop Canada Inc.) 1 h post-phagocytosis for up to 1 h. For pH neutralization of the phagolysosome, macrophages were treated with 1 µM concanamycin A (ConA; Bioshop Canada Inc.) and 10 mM NH_4Cl (Bioshop Canada Inc.) 40 min after the start of phagocytosis. In order to inhibit proteases, cells were incubated with a protease inhibitor cocktail (Sigma-Aldrich) 40 min after phagocytosis, which included 1.0 mM AEBSF, 0.8 µM aprotinin, 40.0 µM bestatin, 14.0 µM E-

64, 20.0 µM leupeptin and 15.0 µM pepstatin A. To inhibit the cytoskeleton and dynamin, macrophages were treated with the following inhibitors 40 min post-phagocytosis: 10 µM nocodazole (Sigma-Aldrich), 10 µM taxol (Sigma-Aldrich), 2 µM cytochalasin D (EMD Millipore, Oakville, ON, Canada), 1 µM jasplakinolide (EMD Millipore) and 5 µM dyngo-4a (Abcam). For clathrin inhibitors, cells were incubated with 10 µM of pitstop 2 (Abcam, Cambridge, MA, USA) or 0.5-2.0 µg/mL ikarugamycin (Sigma-Aldrich) 40 min to 4 h after the start of phagocytosis.

Immunofluorescence and fluorescence labeling

External beads were stained for live-cell imaging by incubating macrophages with Cy2-conjugated anti-human IgG (1:100; Jackson ImmunoResearch Labs, West Grove, PA, USA) for 30 min on ice. For internal staining, PFA-fixed cells were permeabilized with 0.1% Triton X-100 for 20 min with the exception of staining with the LAMP1 antibody, which required permeabilization with ice cold methanol for 5 min instead. Primary antibodies that were diluted in 5% skim milk or 1% BSA solutions were applied for 1 h at RT and included: anti-*Legionella* antibody (1:3000; Public Health Ontario), anti-*E. coli* antibody (1:100, Bio-Rad), anti-LAMP1 (1:200; 1D4B; Developmental Studies Hybridoma Bank, Iowa City, IA) and anti-LAMP2 antibody (1:100; ABL-93; Developmental Studies Hybridoma Bank, Iowa City, IA, USA). Fluorescent secondary antibodies (ThermoFisher Scientific or Bethyl Laboratories, Montgomery, TX, USA) were utilized at a 1:1000 dilution within 5% skim milk or 1% BSA solutions for 1 h at RT. The coverslips were mounted using Dako fluorescence mounting medium (Agilent Technologies, Inc. Mississauga, ON, Canada).

For labelling acidic compartments, cells were stained with Lysotracker Red DND-99 at 1 µM and for 1 h (ThermoFisher Scientific). To label degradative compartments, cells were labelled with Magic Red Cathepsin-L substrate (ImmunoChemistry Technologies, LLC, Bloomington, MN, USA) for 1 h, as per the manufacturer's instructions.

For labeling isolated phagosomes, phagosomes were incubated with the following primary antibodies: anti-LAMP1 (1:200 in PBS) and anti-clathrin heavy chain (1:200 in PBS; D3C6; Cell Signalling Technology, Danvers, MA, USA). Phagosomes were washed 3 times with 0.5 % BSA followed by centrifugation at 2000 xg for 1 min. Fluorescent secondary antibodies were added to the phagosomes at a 1:1000 dilution and incubated for 1 h at room temperature, then phagosomes were washed 3 times with 0.5 % BSA followed by centrifugation at 2000 xg for 1 min. Phagosomes were resuspended in PBS and mounted with Dako mounting medium.

Microscopy

Confocal images were acquired using two different spinning disc confocal microscope systems. The first was a Quorum Wave FX-X1 spinning disc confocal microscope system consisting of an inverted fluorescence microscope (DMI6000B; Leica Microsystems, Concord, ON, Canada) equipped with a Hamamatsu ORCA-R^2 camera and a Hamamatsu EM-CCD camera (Quorum Technologies, Inc., Guelph, ON, Canada). The second was a Quorum Diskovery spinning disc confocal microscope system consisting of an inverted fluorescence microscope (DMi8; Leica) equipped with the Andor Zyla 4.2 Megapixel sCMOS and Andor iXON 897 EMCCD camera (Quorum Technologies, Inc.). We also used an inverted microscope (IX81; Olympus Life Science, Richmond Hill, ON, Canada) equipped with a Rolera-MGI Plus EM-CCD camera (Q

Imaging, Tucson, AZ, USA). The microscope systems were controlled by the MetaMorph acquisition software (Molecular Devices, LLC, San Jose, CA, USA). Images were acquired using a 63x oil immersion objective (1.4 NA), a 40x oil immersion objective (1.3 NA) or a 40x dry objective (0.60 NA). For live-cell imaging, coverslips were imaged in a chamber containing DMEM supplemented with 10% FBS in a microscope-mounted chamber maintained at 37 °C and 5% CO_2.

Image processing and analysis

Image processing and quantitative analysis were performed using FIJI (Schindelin et al., 2012) or Volocity (PerkinElmer, Waltham, MA, USA), where image enhancements were completed without altering the quantitative relationship between image elements. For the quantification of the total volume of *E. coli*-containing phagosomes in each cell, phagosomes were first identified in Volocity by their high fluorescence intensity and then by their volume, set as greater than 1 μm^3. The volume of phagosomes in each cell were added together for each time point and normalized to the first acquisition time point (T_0). For the quantification of the total volume of PDVs containing *E. coli*-derived debris, we had Volocity select dimmer fluorescence objects and then defined their volume as greater than 0.02 μm^3, but less than 5 μm^3. The volume of individual PDVs in each cell were summed and in the case of time-lapse microscopy, normalized to the first time point. Phagosomes were excluded from the PDV quantifications, as the inclusion of lower fluorescence intensities allowed PDVs closely surrounding the phagosome to be included in the phagosome volume, thereby increasing the apparent size of the phagosomes above the volume threshold for PDVs (Supplemental Figure S3). For the quantification of the total volume of *Legionella*-containing phagosomes and PDVs in each cell, we utilized the same

methodology as for *E. coli*, except that the phagosome was included in the quantifications if its volume exceeded 5 μm^3. For the co-occurrence of Lysotracker red or Magic red with PDVs containing *E. coli*-derived debris, we used Manders' colocalization analysis in Volocity, where PDVs were included within this analysis if their surface area was greater than 0.1 μm^2, but less than 4 μm^2. The markers were considered to co-occur when the M_2 colocalization coefficient was determined to be greater than 0.7. We then reported the percentage of PDVs that were positive for Magic red or Lysotracker (co-occurrence of markers).

For the counting of phagosome and PDV events, images of mRFP1-labeled *E. coli* and PDV were first thresholded to exclude background and macrophage autofluorescence signals, and to minimize signal overlap of events while retaining as much low-intensity events as possible. Once an intensity threshold was identified, it was applied to all images of all samples of the same experimental replicate. External events were identified by colocalization with external anti-*E. coli* fluorescence signal and excluded from analysis. The thresholded images were used to create binary images of the samples, and the binary images were processed by object segmentation using FIJI's Watershed function. Intact phagosome events were identified manually by the rod-shaped events characteristic of *E. coli* shape. PDVs between 0.015 μm^2 and 1.2 μm^2 were counted using FIJI's Analyze Particles function.

For the quantification of the number of free lysosomes in each cell, we used Volocity to separate touching objects in the LAMP1 channel using an object size guide of 0.29 μm^3 (determined by assessing the lysosome size in resting macrophages). LAMP1-positive objects were considered free lysosomes if their volume was greater than 0.02 μm^3, but less than 5 μm^3 and they were not touching the filament-containing phagolysosomes (applied a mask to the

filament). The treatments were finally normalized to the "no-phagocytosis" group, which was considered to contain 100% free lysosomes.

For the determination of presence and absence of LAMP1 and LAMP2 on PDVs, first, PDVs in an image were identified as vesicles with an image area between 0.015 μm^2 and 1.2 μm^2. Then PDVs were assessed for the presence of absence of LAMP1 or LAMP2 colocalized to the PDV, and cells are scored by percentage of PDVs with colocalized LAMP1 or LAMP2 fluorescent signal. For the determination of phagosome mixing, images of second-wave phagosomes and fragments (GFP) were thresholded to exclude background and macrophage autofluorescence signals, then a binary mask was formed.

Second-wave events external to the cell were determined by comparison to Brightfield images and excluded from the mask. The mean fluorescence intensity of first-wave phagosome remnants (mRFP1) colocalized to the second-wave mask was determined and corrected by numerical subtraction of mean background intensity. For the determination of DQ-BSA intensity, images in a stack corresponding to the lower half of DQ-BSA beads were collapsed by Maximum Intensity Projection (MIP), and the MIP images were thresholded to exclude non-DQ-BSA bead events. External beads were identified by colocalization of Cy2-anti-human fluorescence signal and excluded from analysis by Cy2 mask subtraction. Following mask subtraction, DQ-BSA proteolytic activity was determined by measuring the mean fluorescence of internalized beads and corrected by numerical subtraction of mean external DQ-BSA bead intensity. Deconvolution (30 iterations) was performed utilizing Volocity software. Figures were assembled using Adobe Illustrator (Adobe Systems, Inc., San Jose, CA, USA).

Statistical analysis

Data was presented as mean ± SEM of at least three independent experiments unless otherwise stated. The numbers of cells assessed in each experiment is indicated within the figure legends. Statistical analysis was performed using GraphPad Prism software (GraphPad Software, Inc., San Diego, CA, USA). An unpaired, two-tailed Student's t-test was utilized to compare two conditions, while multiple conditions were compared using a one-way ANOVA with Tukey's *post hoc* test, a two-way ANOVA with Tukey's *post hoc* test or a two-way ANOVA with Sidak's *post hoc* test. Curves were fit to the data using non-linear regression, where AIC was used to select the model that best fit the data. The slopes of the lines using linear regression were statistically compared using an ANCOVA. In any of the statistical tests performed, values of $p < 0.05$ were considered significant.

References

Aderem, A. 2002. How to Eat Something Bigger than Your Head. *Cell*. 110:5–8. doi:10.1016/S0092-8674(02)00819-X.

Aguet, F., C.N. Antonescu, M. Mettlen, S.L. Schmid, and G. Danuser. 2013. Advances in analysis of low signal-to-noise images link dynamin and AP2 to the functions of an endocytic checkpoint. *Dev. Cell*. 26:279–291. doi:10.1016/j.devcel.2013.06.019.

Alvarez, M., and A. Casadevall. 2006. Phagosome Extrusion and Host-Cell Survival after Cryptococcus neoformans Phagocytosis by Macrophages. *Curr. Biol.* 16:2161–2165. doi:10.1016/j.cub.2006.09.061.

Arneson, L.S., J. Kunz, R.A. Anderson, and L.M. Traub. 1999. Coupled inositide phosphorylation and phospholipase D activation initiates clathrin-coat assembly on lysosomes. *J. Biol. Chem.* 274:17794–805. doi:10.1074/jbc.274.25.17794.

Bezanilla, M., A.S. Gladfelter, D.R. Kovar, and W.-L. Lee. 2015. Cytoskeletal dynamics: A view from the membrane. *J. Cell Biol.* 209:329–337. doi:10.1083/jcb.201502062.

Borgne, R. Le, and B. Hoflack. 1997. Mannose 6-Phosphate Receptors Regulate the Formation of Clathrin-coated Vesicles in the TGN. *J. Cell Biol.* 137:335–345. doi:10.1083/jcb.137.2.335.

Botelho, R.J., D.J. Hackam, A.D. Schreiber, and S. Grinstein. 2000. Role of COPI in Phagosome Maturation. *J. Biol. Chem.* 275:15717–15727. doi:10.1074/jbc.M910068199.

Brassinga, A.K.C., J.M. Kinchen, M.E. Cupp, S.R. Day, P.S. Hoffman, and C.D. Sifri. 2010. Caenorhabditis is a metazoan host for Legionella. *Cell. Microbiol.* 12:343–361.

doi:10.1111/j.1462-5822.2009.01398.x.

Campbell, R.E., O. Tour, A.E. Palmer, P.A. Steinbach, G.S. Baird, D.A. Zacharias, and R.Y. Tsien. 2002. A monomeric red fluorescent protein. *Proc. Natl. Acad. Sci. U. S. A.* 99:7877–7882. doi:10.1073/pnas.082243699.

Cannon, G.J., and J.A. Swanson. 1992. The macrophage capacity for phagocytosis. *J. Cell Sci.* 101 (Pt 4:907–13.

Chantranupong, L., S.M. Scaria, R.A. Saxton, M.P. Gygi, K. Shen, G.A. Wyant, T. Wang, J.W. Harper, S.P. Gygi, and D.M. Sabatini. 2016. The CASTOR Proteins Are Arginine Sensors for the mTORC1 Pathway. *Cell*. 165:153–164. doi:10.1016/j.cell.2016.02.035.

Clarke, M., J. Köhler, Q. Arana, T. Liu, J. Heuser, and G. Gerisch. 2002. Dynamics of the vacuolar H(+)-ATPase in the contractile vacuole complex and the endosomal pathway of Dictyostelium cells. *J. Cell Sci.* 115:2893–905.

Curchoe, C.L., and U. Manor. 2017. Actin Cytoskeleton-Mediated Constriction of Membrane Organelles via Endoplasmic Reticulum Scaffolding. *ACS Biomater. Sci. Eng.* 3:2727–2732. doi:10.1021/acsbiomaterials.6b00802.

Damiani, M. 2003. Microfilaments and microtubules regulate recycling from phagosomes. *Exp. Cell Res.* 289:152–161. doi:10.1016/S0014-4827(03)00253-2.

Delevoye, C., S. Miserey-Lenkei, G. Montagnac, F. Gilles-Marsens, P. Paul-Gilloteaux, F. Giordano, F. Waharte, M.S. Marks, B. Goud, and G. Raposo. 2014. Recycling Endosome Tubule Morphogenesis from Sorting Endosomes Requires the Kinesin Motor KIF13A. *Cell Rep.* 6:445–454. doi:10.1016/j.celrep.2014.01.002.

Dong, R., Y. Saheki, S. Swarup, L. Lucast, J.W. Harper, and P. De Camilli. 2016. Endosome-ER Contacts Control Actin Nucleation and Retromer Function through VAP-Dependent Regulation of PI4P. *Cell*. 166:408–423. doi:10.1016/j.cell.2016.06.037.

Du, W., Q.P. Su, Y. Chen, Y. Zhu, D. Jiang, Y. Rong, S. Zhang, Y. Zhang, H. Ren, C. Zhang, X. Wang, N. Gao, Y. Wang, L. Sun, Y. Sun, and L. Yu. 2016. Kinesin 1 Drives Autolysosome Tubulation. *Dev. Cell*. 37:326–336. doi:10.1016/j.devcel.2016.04.014.

Fairn, G.D., and S. Grinstein. 2012. How nascent phagosomes mature to become phagolysosomes. *Trends Immunol.* 33:397–405. doi:10.1016/j.it.2012.03.003.

Fratti, R.A., J.M. Backer, J. Gruenberg, S. Corvera, and V. Deretic. 2001. Role of phosphatidylinositol 3-kinase and Rab5 effectors in phagosomal biogenesis and mycobacterial phagosome maturation arrest. *J. Cell Biol.* 154:631–644. doi:10.1083/jcb.200106049.

van Furth, R., and Z.A. Cohn. 1968. The origin and kinetics of mononuclear phagocytes. *J. Exp. Med.* 128:415–35. doi:10.1084/jem.128.3.415.

Gan, Q., X. Wang, Q. Zhang, Q. Yin, Y. Jian, Y. Liu, N. Xuan, J. Li, J. Zhou, K. Liu, Y. Jing, X. Wang, and C. Yang. 2019. The amino acid transporter SLC-36.1 cooperates with PtdIns3P 5-kinase to control phagocytic lysosome reformation. *J. Cell Biol.* 218:2619–2637. doi:10.1083/jcb.201901074.

Garg, S., M. Sharma, C. Ung, A. Tuli, D.C. Barral, D.L. Hava, N. Veerapen, G.S. Besra, N. Hacohen, and M.B. Brenner. 2011. Lysosomal Trafficking, Antigen Presentation, and Microbial Killing Are Controlled by the Arf-like GTPase Arl8b. *Immunity*. 35:182–193. doi:10.1016/j.immuni.2011.06.009.

Gautreau, A., K. Oguievetskaia, and C. Ungermann. 2014. Function and Regulation of the Endosomal Fusion and Fission Machineries. *Cold Spring Harb. Perspect. Biol.* 6:a016832–a016832. doi:10.1101/cshperspect.a016832.

Gotthardt, D., H.J. Warnatz, O. Henschel, F. Brückert, M. Schleicher, and T. Soldati. 2002. High-Resolution Dissection of Phagosome Maturation Reveals Distinct Membrane Trafficking Phases. *Mol. Biol. Cell*. 13:3508–3520. doi:10.1091/mbc.e02-04-0206.

Gray, M., and R.J. Botelho. 2017. Phagocytosis and Phagosomes. 1519. R. Botelho, editor. Springer New York, New York, NY. 1–16 pp.

Gray, M.A., C.H. Choy, R.M. Dayam, E. Ospina-Escobar, A. Somerville, X. Xiao, S.M. Ferguson, and R.J. Botelho. 2016. Phagocytosis Enhances Lysosomal and Bactericidal Properties by Activating the Transcription Factor TFEB. *Curr. Biol.* 26:1955–1964. doi:10.1016/j.cub.2016.05.070.

Gutierrez, M.G. 2013. Functional role(s) of phagosomal Rab GTPases. *Small GTPases*. 4:148–158. doi:10.4161/sgtp.25604.

Harding, C. V., and H.J. Geuze. 1992. Class II MHC molecules are present in macrophage lysosomes and phagolysosomes that function in the phagocytic processing of Listeria monocytogenes for presentation to T cells. *J. Cell Biol.* 119:531–542. doi:10.1083/jcb.119.3.531.

Harrison, R.E., C. Bucci, O. V. Vieira, T.A. Schroer, and S. Grinstein. 2003. Phagosomes Fuse with Late Endosomes and/or Lysosomes by Extension of Membrane Protrusions along Microtubules: Role of Rab7 and RILP. *Mol. Cell. Biol.* 23:6494–6506. doi:10.1128/MCB.23.18.6494-6506.2003.

Hazeki, K., K. Nigorikawa, Y. Takaba, T. Segawa, A. Nukuda, A. Masuda, Y. Ishikawa, K. Kubota, S. Takasuga, and O. Hazeki. 2012. Essential roles of PIKfyve and PTEN on phagosomal phosphatidylinositol 3-phosphate dynamics. *FEBS Lett.* 586:4010–4015. doi:10.1016/j.febslet.2012.09.043.

Henson, P.M. 2017. Cell Removal: Efferocytosis. *Annu. Rev. Cell Dev. Biol.* 33:127–144. doi:10.1146/annurev-cellbio-111315-125315.

Hipolito, V.E.B., J.A. Diaz, K. V. Tandoc, C. Oertlin, J. Ristau, N. Chauhan, A. Saric, S. McLaughlan, O. Larsson, I. Topisirovic, and R.J. Botelho. 2019. Enhanced translation expands the endo-lysosome size and promotes antigen presentation during phagocyte activation. *PLoS Biol.* 17. doi:10.1371/journal.pbio.3000535.

Hoyer, M.J., P.J. Chitwood, C.C. Ebmeier, J.F. Striepen, R.Z. Qi, W.M. Old, and G.K. Voeltz. 2018. A Novel Class of ER Membrane Proteins Regulates ER-Associated Endosome Fission. *Cell*. 175:254-265.e14. doi:10.1016/j.cell.2018.08.030.

Inpanathan, S., and R.J. Botelho. 2019. The Lysosome Signaling Platform: Adapting With the Times. *Front. Cell Dev. Biol.* 7:113. doi:10.3389/fcell.2019.00113.

Jans, R., M. Sartor, M. Jadot, and Y. Poumay. 2004. Calcium entry into keratinocytes induces exocytosis of lysosomes. *Arch. Dermatol. Res.* 296:30–41. doi:10.1007/s00403-004-0469-0.

Jeschke, A., and A. Haas. 2018. Sequential actions of phosphatidylinositol phosphates regulate phagosome-lysosome fusion. *Mol. Biol. Cell*. 29:452–465. doi:10.1091/mbc.E17-07-0464.

Jordens, I., M. Fernandez-Borja, M. Marsman, S. Dusseljee, L. Janssen, J. Calafat, H. Janssen, R. Wubbolts, and J. Neefjes. 2001. The Rab7 effector protein RILP controls lysosomal transport by inducing the recruitment of dynein-dynactin motors. *Curr. Biol.* 11:1680–1685. doi:10.1016/S0960-9822(01)00531-0.

Katayama, H., A. Yamamoto, N. Mizushima, T. Yoshimori, and A. Miyawaki. 2008. GFP-like Proteins Stably Accumulate in Lysosomes. *Cell Struct. Funct.* 33:1–12. doi:10.1247/csf.07011.

Kim, G.H.E., R.M. Dayam, A. Prashar, M. Terebiznik, and R.J. Botelho. 2014. PIKfyve

Inhibition Interferes with Phagosome and Endosome Maturation in Macrophages. *Traffic*. 15:1143–1163. doi:10.1111/tra.12199.

Kinchen, J.M., and K.S. Ravichandran. 2010. Identification of two evolutionarily conserved genes regulating processing of engulfed apoptotic cells. *Nature*. 464:778–782. doi:10.1038/nature08853.

Kirchhausen, T., D. Owen, and S.C. Harrison. 2014. Molecular structure, function, and dynamics of clathrin-mediated membrane traffic. *Cold Spring Harb. Perspect. Biol.* 6:a016725–a016725. doi:10.1101/cshperspect.a016725.

Krajcovic, M., S. Krishna, L. Akkari, J.A. Joyce, and M. Overholtzer. 2013. mTOR regulates phagosome and entotic vacuole fission. *Mol. Biol. Cell*. 24:3736–3745. doi:10.1091/mbc.e13-07-0408.

Krishna, S., W. Palm, Y. Lee, W. Yang, U. Bandyopadhyay, H. Xu, O. Florey, C.B. Thompson, and M. Overholtzer. 2016. PIKfyve Regulates Vacuole Maturation and Nutrient Recovery following Engulfment. *Dev. Cell.* 38:536–547. doi:10.1016/j.devcel.2016.08.001.

Lancaster, C.E., C.Y. Ho, V.E.B. Hipolito, R.J. Botelho, and M.R. Terebiznik. 2019. Phagocytosis: what's on the menu? *Biochem. Cell Biol*. 97:21–29. doi:10.1139/bcb-2018-0008.

Levin-Konigsberg, R., F. Montaño-Rendón, T. Keren-Kaplan, R. Li, B. Ego, S. Mylvaganam, J.E. DiCiccio, W.S. Trimble, M.C. Bassik, J.S. Bonifacino, G.D. Fairn, and S. Grinstein. 2019. Phagolysosome resolution requires contacts with the endoplasmic reticulum and phosphatidylinositol-4-phosphate signalling. *Nat. Cell Biol.* 21:1234–1247. doi:10.1038/s41556-019-0394-2.

Levin, R., S. Grinstein, and J. Canton. 2016. The life cycle of phagosomes: formation, maturation, and resolution. *Immunol. Rev.* 273:156–179. doi:10.1111/imr.12439.

Levin, R., G.R.V. V Hammond, T. Balla, P. De Camilli, G.D. Fairn, and S. Grinstein. 2017. Multiphasic dynamics of phosphatidylinositol 4-phosphate during phagocytosis. *Mol. Biol. Cell*. 28:128–140. doi:10.1091/mbc.e16-06-0451.

Li, M., B. Khambu, H. Zhang, J.-H. Kang, X. Chen, D. Chen, L. Vollmer, P.-Q. Liu, A. Vogt, and X.-M. Yin. 2013. Suppression of Lysosome Function Induces Autophagy via a Feedback Down-regulation of MTOR Complex 1 (MTORC1) Activity. *J. Biol. Chem.* 288:35769–35780. doi:10.1074/jbc.M113.511212.

Liebl, D., and G. Griffiths. 2009. Transient assembly of F-actin by phagosomes delays phagosome fusion with lysosomes in cargo-overloaded macrophages. *J. Cell Sci.* 122:2935–2945. doi:10.1242/jcs.048355.

Ludwig, T., H. Munier-Lehmann, U. Bauer, M. Hollinshead, C. Ovitt, P. Lobel, and B. Hoflack. 1994. Differential sorting of lysosomal enzymes in mannose 6-phosphate receptor-deficient fibroblasts. *EMBO J.* 13:3430–3437. doi:10.1002/j.1460-2075.1994.tb06648.x.

Ma, H., J.E. Croudace, D.A. Lammas, and R.C. May. 2006. Expulsion of Live Pathogenic Yeast by Macrophages. *Curr. Biol.* 16:2156–2160. doi:10.1016/j.cub.2006.09.032.

Maniak, M. 2003. Fusion and Fission Events in the Endocytic Pathway of Dictyostelium. *Traffic*. 4:1–5. doi:10.1034/j.1600-0854.2003.40101.x.

Mantegazza, A.R., J.G. Magalhaes, S. Amigorena, and M.S. Marks. 2013. Presentation of Phagocytosed Antigens by MHC Class I and II. *Traffic*. 14:135–152. doi:10.1111/tra.12026.

Mantegazza, A.R., A.L. Zajac, A. Twelvetrees, E.L.F. Holzbaur, S. Amigorena, and M.S. Marks. 2014. TLR-dependent phagosome tubulation in dendritic cells promotes phagosome cross-talk to optimize MHC-II antigen presentation. *Proc. Natl. Acad. Sci.* 111:15508–15513.

doi:10.1073/pnas.1412998111.

Mettlen, M., T. Pucadyil, R. Ramachandran, and S.L. Schmid. 2009. Dissecting dynamin's role in clathrin-mediated endocytosis. *Biochem. Soc. Trans.* 37:1022–1026. doi:10.1042/BST0371022.

Mrakovic, A., J.G. Kay, W. Furuya, J.H. Brumell, and R.J. Botelho. 2012. Rab7 and Arl8 GTPases are Necessary for Lysosome Tubulation in Macrophages. *Traffic*. 13:1667–1679. doi:10.1111/tra.12003.

Munson, M.J., G.F. Allen, R. Toth, D.G. Campbell, J.M. Lucocq, and I.G. Ganley. 2015. mTOR activates the VPS 34– UVRAG complex to regulate autolysosomal tubulation and cell survival. *EMBO J.* 34:2272–2290. doi:10.15252/embj.201590992.

Naufer, A., V.E.B. Hipolito, S. Ganesan, A. Prashar, V. Zaremberg, R.J. Botelho, and M.R. Terebiznik. 2018. pH of endophagosomes controls association of their membranes with Vps34 and PtdIns(3)P levels. *J. Cell Biol.* 217:329–346. doi:10.1083/jcb.201702179.

Niedergang, F., and S. Grinstein. 2018. How to build a phagosome: new concepts for an old process. *Curr. Opin. Cell Biol.* 50:57–63. doi:10.1016/j.ceb.2018.01.009.

Parihar, A., T.D. Eubank, and A.I. Doseff. 2010. Monocytes and Macrophages Regulate Immunity through Dynamic Networks of Survival and Cell Death. *J. Innate Immun.* 2:204–215. doi:10.1159/000296507.

Pauwels, A.-M., M. Trost, R. Beyaert, and E. Hoffmann. 2017. Patterns, Receptors, and Signals: Regulation of Phagosome Maturation. *Trends Immunol.* 38:407–422. doi:10.1016/j.it.2017.03.006.

Prashar, A., S. Bhatia, D. Gigliozzi, T. Martin, C. Duncan, C. Guyard, and M.R. Terebiznik. 2013. Filamentous morphology of bacteria delays the timing of phagosome morphogenesis in macrophages. *J. Cell Biol.* 203:1081–1097. doi:10.1083/jcb.201304095.

Prashar, A., and M.R. Terebiznik. 2015. Legionella pneumophila: homeward bound away from the phagosome. *Curr. Opin. Microbiol.* 23:86–93. doi:10.1016/j.mib.2014.11.008.

Ramachandra, L., R. Song, and C. V Harding. 1999. Phagosomes are fully competent antigen-processing organelles that mediate the formation of peptide:class II MHC complexes. *J. Immunol.* 162:3263–72.

Rink, J., E. Ghigo, Y. Kalaidzidis, and M. Zerial. 2005. Rab Conversion as a Mechanism of Progression from Early to Late Endosomes. *Cell*. 122:735–749. doi:10.1016/j.cell.2005.06.043.

Ripoll, L., X. Heiligenstein, I. Hurbain, L. Domingues, F. Figon, K.J. Petersen, M.K. Dennis, A. Houdusse, M.S. Marks, G. Raposo, and C. Delevoye. 2018. Myosin VI and branched actin filaments mediate membrane constriction and fission of melanosomal tubule carriers. *J. Cell Biol.* 217:2709–2726. doi:10.1083/jcb.201709055.

Roberts, R.L., M.A. Barbieri, J. Ullrich, and P.D. Stahl. 2000. Dynamics of rab5 activation in endocytosis and phagocytosis. *J. Leukoc. Biol.* 68:627–32. doi:10.1189/jlb.68.5.627.

Rong, Y., M. Liu, L. Ma, W. Du, H. Zhang, Y. Tian, Z. Cao, Y. Li, H. Ren, C. Zhang, L. Li, S. Chen, J. Xi, and L. Yu. 2012. Clathrin and phosphatidylinositol-4,5-bisphosphate regulate autophagic lysosome reformation. *Nat. Cell Biol.* 14:924–934. doi:10.1038/ncb2557.

Rowland, A.A., P.J. Chitwood, M.J. Phillips, and G.K. Voeltz. 2014. ER contact sites define the position and timing of endosome fission. *Cell*. 159:1027–1041. doi:10.1016/j.cell.2014.10.023.

Saffi, G.T., and R.J. Botelho. 2019. Lysosome Fission: Planning for an Exit. *Trends Cell Biol.* 29:635–646. doi:10.1016/j.tcb.2019.05.003.

Saric, A., V.E.B. Hipolito, J.G. Kay, J. Canton, C.N. Antonescu, and R.J. Botelho. 2016. mTOR controls lysosome tubulation and antigen presentation in macrophages and dendritic cells. *Mol. Biol. Cell*. 27:321–333. doi:10.1091/mbc.e15-05-0272.

Saxton, R.A., L. Chantranupong, K.E. Knockenhauer, T.U. Schwartz, and D.M. Sabatini. 2016. Mechanism of arginine sensing by CASTOR1 upstream of mTORC1. *Nature*. 536:229–233. doi:10.1038/nature19079.

Schindelin, J., I. Arganda-Carreras, E. Frise, V. Kaynig, M. Longair, T. Pietzsch, S. Preibisch, C. Rueden, S. Saalfeld, B. Schmid, J.Y. Tinevez, D.J. White, V. Hartenstein, K. Eliceiri, P. Tomancak, and A. Cardona. 2012. Fiji: An open-source platform for biological-image analysis. *Nat. Methods*. 9:676–682. doi:10.1038/nmeth.2019.

Sridhar, S., B. Patel, D. Aphkhazava, F. Macian, L. Santambrogio, D. Shields, and A.M. Cuervo. 2013. The lipid kinase PI4KIIIβ preserves lysosomal identity. *EMBO J.* 32:324–339. doi:10.1038/emboj.2012.341.

Stewart, J.R., and R.A. Weisman. 1972. Exocytosis of latex beads during the encystment of Acanthamoeba. *J. Cell Biol.* 52:117–30. doi:10.1083/jcb.52.1.117.

Stoorvogel, W., V. Oorschot, and H.J. Geuze. 1996. A novel class of clathrin-coated vesicles budding from endosomes. *J. Cell Biol.* 132:21–33. doi:10.1083/jcb.132.1.21.

Swanson, J. a, M.T. Johnson, K. Beningo, P. Post, M. Mooseker, and N. Araki. 1999. A contractile activity that closes phagosomes in macrophages. *J. Cell Sci.* 112 (Pt 3:307–16.

Traub, L.M., S.I. Bannykh, J.E. Rodel, M. Aridor, W.E. Balch, and S. Kornfeld. 1996. AP-2-containing clathrin coats assemble on mature lysosomes. *J. Cell Biol.* 135:1801–1814. doi:10.1083/jcb.135.6.1801.

Vieira, O. V., R.J. Botelho, L. Rameh, S.M. Brachmann, T. Matsuo, H.W. Davidson, A. Schreiber, J.M. Backer, L.C. Cantley, and S. Grinstein. 2001. Distinct roles of class I and class III phosphatidylinositol 3-kinases in phagosome formation and maturation. *J. Cell Biol.* 155:19–26. doi:10.1083/jcb.200107069.

Vieira, O. V., C. Bucci, R.E. Harrison, W.S. Trimble, L. Lanzetti, J. Gruenberg, A.D. Schreiber, P.D. Stahl, and S. Grinstein. 2003. Modulation of Rab5 and Rab7 Recruitment to Phagosomes by Phosphatidylinositol 3-Kinase. *Mol. Cell. Biol.* 23:2501–2514. doi:10.1128/MCB.23.7.2501-2514.2003.

Vieira, O. V, R.E. Harrison, C.C. Scott, H. Stenmark, D. Alexander, J. Liu, J. Gruenberg, A.D. Schreiber, and S. Grinstein. 2004. Acquisition of Hrs, an Essential Component of Phagosomal Maturation, Is Impaired by Mycobacteria. *Mol. Cell. Biol.* 24:4593–4604. doi:10.1128/MCB.24.10.4593-4604.2004.

Visvikis, O., N. Ihuegbu, S.A. Labed, L.G. Luhachack, A.-M.F. Alves, A.C. Wollenberg, L.M. Stuart, G.D. Stormo, and J.E. Irazoqui. 2014. Innate Host Defense Requires TFEB-Mediated Transcription of Cytoprotective and Antimicrobial Genes. *Immunity*. 40:896–909. doi:10.1016/j.immuni.2014.05.002.

Vyas, J.M., Y.-M. Kim, K. Artavanis-Tsakonas, J.C. Love, A.G. Van der Veen, and H.L. Ploegh. 2007. Tubulation of Class II MHC Compartments Is Microtubule Dependent and Involves Multiple Endolysosomal Membrane Proteins in Primary Dendritic Cells. *J. Immunol.* 178:7199–7210. doi:10.4049/jimmunol.178.11.7199.

Werb, Z., and Z.A. Cohn. 1972. Plasma membrane synthesis in the macrophage following phagocytosis of polystyrene latex particles. *J. Biol. Chem.* 247:2439–46.

Wu, X.-S., S.H. Lee, J. Sheng, Z. Zhang, W.-D. Zhao, D. Wang, Y. Jin, P. Charnay, J.M. Ervasti, and L.-G. Wu. 2016. Actin Is Crucial for All Kinetically Distinguishable Forms of

Endocytosis at Synapses. *Neuron*. 92:1020–1035. doi:10.1016/j.neuron.2016.10.014.

Xu, J., K.A. Toops, F. Diaz, J.M. Carvajal-Gonzalez, D. Gravotta, F. Mazzoni, R. Schreiner, E. Rodriguez-Boulan, and A. Lakkaraju. 2013. Mechanism of polarized lysosome exocytosis in epithelial cells. *J. Cell Sci.* 126:5086–5086. doi:10.1242/jcs.143982.

Yasuda, S., S. Morishita, A. Fujita, T. Nanao, N. Wada, S. Waguri, G. Schiavo, M. Fukuda, and T. Nakamura. 2016. Mon1–Ccz1 activates Rab7 only on late endosomes and dissociates from the lysosome in mammalian cells. *J. Cell Sci.* 129:329–340. doi:10.1242/jcs.178095.

Yu, L., C.K. McPhee, L. Zheng, G.A. Mardones, Y. Rong, J. Peng, N. Mi, Y. Zhao, Z. Liu, F. Wan, D.W. Hailey, V. Oorschot, J. Klumperman, E.H. Baehrecke, and M.J. Lenardo. 2010. Termination of autophagy and reformation of lysosomes regulated by mTOR. *Nature*. 465:942–946. doi:10.1038/nature09076.

Zent, C.S., and M.R. Elliott. 2017. Maxed out macs: physiologic cell clearance as a function of macrophage phagocytic capacity. *FEBS J.* 284:1021–1039. doi:10.1111/febs.13961.

Zoncu, R., L. Bar-Peled, A. Efeyan, S. Wang, Y. Sancak, and D.M. Sabatini. 2011. mTORC1 Senses Lysosomal Amino Acids Through an Inside-Out Mechanism That Requires the Vacuolar H+-ATPase. *Science (80-.).* 334:678–683. doi:10.1126/science.1207056.

Figure Legends

Figure 1. Phagolysosomes do not undergo exocytosis. A and **C**: RAW macrophages were presented with IgG-opsonized beads and then tracked for 24 h (A) or exposed to 10 µM ionomycin and 1.2 mM of Ca^{2+} (C). Shown are single z-plane DIC images. Scale bars (A): main panels at 10 µm; insets at 5 µm and the coloured boxes indicate the positions of the insets. Scale bars (C): 10 µm. In either experiment, we did not observe exocytosis of phagosomes. **B** and **C.** The number of latex beads within macrophages after indicated chase period and normalized to the measurement (T_0). All data shown as mean ± SEM from three independent experiments, were 8 cells (B) and 10 cells (D) were quantified per independent experiment. Conditions were compared statistically using a one-way ANOVA with Tukey's post-hoc test – no statistical difference was observed. See videos 1 and 2 for corresponding movies.

Figure 2. Phagolysosomes undergo fragmentation. A, B and **D.** RAW macrophages were challenged with IgG-opsonized, filamentous mCherry-*Legionella* for 7 h (A) or with IgG-opsonized mRFP1-*E. coli* for 2 h (B, D) and then imaged live. A,B: The main panels show the red channel in a rainbow scale, where red and blue are the highest and lowest intensity levels, respectively. The smaller panels show the red and DIC channels for the first frame. A, B, and D: White dashed lines indicate the boundary of the cell. **C.** The total volume of phagosomes and PDVs present within each cell over time (see Sup. Fig. S3 for details), shown as mean ± SEM of 3 independent experiments. Volume was normalized to the first measurement (T_0), where 10 cells to 25 cells were quantified for each independent experiment **E.** Quantification of the number of PDVs and intact phagosomes. Data are represented as means ± SEM of 3 independent experiments, where 15 images were quantified per time point. For C and E: a one-way ANOVA with Tukey's post-hoc test was employed to compare each time point against the 0 h time point (*, $p < 0.05$; ns, not significant). See videos 3 and 4 for corresponding movies. Scale bar for all panels: 10 µm.

Figure 3. Phagosomes undergo different modes of membrane fission. RAW macrophages were allowed to engulf mRFP1-*E. coli* for 1 h, followed by a 3 h chase to elicit phagosome fragmentation. Cells were then subject to live-cell imaging for 10-min intervals, acquiring 1 frame every 3 s. We captured vesicle budding events both from phagosomes that had yet collapsed the rod shape of the *E. coli* cargo (early budding) or after initiating fragmentation (late budding), tubulation that either resulted in a fragment or collapsed back into the phagosome (shown), and apparent constriction events forming large fragments rather than small vesicles.

Red arrows track single events described above. See videos 4, 5, 6 and 7 for corresponding live-imaging. Scale bar = 2 µm.

Figure 4: Fragmentation of the phagolysosome requires cargo degradation and the cytoskeleton. A, C, E and **G.** Neutralization of phagosomal pH (A), protease inhibition (C), microtubule disruption (E) and actin disruption (G) all prevented fragmentation of the phagolysosome. After phagocytosis and treatment with concanamycin A (ConA; 1 µM) and NH_4Cl (10 mM) (A), protease inhibitor cocktail (C), microtubule inhibitors (E), actin inhibitors (G), or vehicle control (DMSO, all conditions), cells were fixed 1 and 4 h post-phagocytosis and immunostained against *E. coli*. The antibody staining of *E. coli* is displayed in a rainbow scale, where red is the highest intensity level and blue is the lowest intensity level. The white dotted lines indicate the boundary of the cells. Scale bar: 5 µm. **B, D, F,** and **H.** The total volume of PDVs was quantified per cell for indicated treatments (see Sup. Fig. S3 for details). Data are represented as mean ± SEM of 3 independent experiments, where 25 cells were quantified for each control/treatment per independent experiment and compared statistically using a one-way ANOVA with Tukey's post-hoc test, where conditions with different letters are considered statistically different ($p < 0.05$).

Figure 5. Clathrin localizes to the phagolysosome. A and **C.** Macrophages expressing clathrin light chain-GFP were allowed to internalize IgG-opsonized beads (A; internal beads marked with *) or mCherry-Legionella (C). Macrophages were incubated for 3-8 h before live cell imaging. For A: colour scale indicates the fluorescence intensity of clathrin-GFP. Time interval between

frames is 10 sec. Green arrows indicate accumulation of clathrin light chain on the surface of phagosomes, which persists for at least 30 sec on the phagosome surface indicating association with the organelle. Scale bar = 5 µm. For c**.** collapsed z-stacks are shown, while insets are deconvolved, single z-planes. White boxes denote the position of the insets. Arrows indicate areas where clathrin is in close association with *Legionella*. Scale bars: main panels = 10 µm; large insets = 0.5 µm; smaller insets = 0.1 µm. **B.** Isolated and fixed phagosomes (indicated by *) were immunolabeled with LAMP-1 (red) and clathrin (green) antibodies. Top row: a z-stack of a single phagosome projected as the Maximum Intensity Projection, displaying a clathrin patch on top a phagosome. Middle row: single-plane image of isolated phagosome showing clathrin patches. Bottom row: cluster of phagosomes co-isolated. Images are representative of 24 phagosomes analyzed. Scale bar = 2 µm.

Figure 6. Clathrin is necessary for the resolution of the phagolysosome. A and **C.** Macrophages were challenged with mCherry-*Legionella* filaments (A) or mCherry-E. coli (C). For A, cells were imaged live 4 h after phagocytosis. Inhibitors were added 10 minutes before the start of imaging. For C, cells were fixed after indicated times and imaged. Image representation is as described before. Scale bar: 5 µm. **B.** Quantification of the volume of phagosomes and PDVs within vehicle-treated cells and pitstop-treated cells as described in Sup. Fig. S3. The volume was normalized to the first measurement (T_0) for the respective treatment. Data are presented as the mean ± SEM of 3 independent experiments and * $p < 0.05$ indicates that the slopes of the regression lines are significantly different. **D.** The total volume of PDVs per cell for experiments shown in C. Data is represented as mean ± SEM of 3 independent experiments, where 25 cells were quantified for each control/treatment per independent

experiment. Conditions were compared statistically using a one-way ANOVA with Tukey's post-hoc test, where conditions with different letters are considered statistically different ($p < 0.05$). **E.** Macrophages were allowed to internalize mRFP1-*E. coli* for 1 h before treatment with indicated compounds. Live-imaging commenced after uptake (0 h) or 6 or 8 h after phagocytosis. Scale bar = 10 µm. **F.** Intact phagosomes and PDVs per cell were quantified as quanta (particle number) for experiments displayed in E. and normalized to 0 h. Data shown as mean ± SEM of 15 images per control/treatment across 3 independent experiments, where each image display 8 to 29 cells. Control and inhibitor-treated cells at each time point were compared statistically using a two-way ANOVA with Sidak's post-hoc test (*, $p < 0.05$; ns, not significant).

Figure 7. Phagosome-derived vesicles exhibit lysosomal properties. A. Macrophages were challenged with ZsGreen-*E. coli* for 6 h prior to fixation and immunostaining against LAMP1 or LAMP2. White dotted lines indicate the boundary of the cells, while arrows indicate colocalization of LAMP1 or LAMP2 to PDVs. Scale bars: main panels = 5 µm; insets = 1 µm. **B.** Quantification of the percentage of PDVs that were positive for LAMP1 or LAMP2. Data are shown as mean ± SD of 60 cells across 3 independent experiments. **C** and **E.** PDVs were generated within macrophages through the fission of ZsGreen-*E. coli* phagosomes at the indicated time points. Cells were then stained with LysoTracker Red (C) or Magic Red cathepsin L substrate (E) for 1 h prior to live-cell imaging. Scale bar = 10 µm. **D** and **F.** PDVs were quantified for co-occurrence with Lysotracker (C) or Magic Red (E). See methods for details. Data are represented as mean ± SEM of 3 independent experiments, where 5 images each containing 5-12 cells were quantified for early and late time points per independent experiment. Time points were compared statistically using an unpaired t-test (* $p < 0.05$).

Figure 8: Phagosome maturation reduces the number of free lysosomes. A and **C.** Macrophages were presented with IgG-beads (A) or mCherry-Legionella (C, Lp), chased for indicated times, fixed, and immunostained for LAMP1. Images show distribution of LAMP1 in resting macrophages or after phagosome maturation (A, C) and *Legionella* (C). Scale bar = 10 µm (A) and 5 µm (C). **B.** Quantification of the number of free lysosomes per cell at the indicated time points after phagocytosis. Lysosomes were considered "free" if they were not fused with the bead phagosome and were found as puncta. **D.** The number of free lysosomes per cell was quantified from images describe in C. Lysosomes were considered "free" if 0.02 μm^3 < volume < 5 μm^3. Data was normalized to resting macrophages. For B and D: Data are represented as mean ± SEM of 3 independent experiments, where 60 cells (B) and 20 cells (D) were quantified for each control/treatment per independent experiment and statistically tested as before.

Figure 9. Phagosomal fragments fuse with subsequent phagosomes. A. Macrophages phagocytosed -*Legionella* for 6 h. A second round of phagocytosis with IgG-opsonized latex beads was then allowed for 1 h before fixation and immunostained against *Legionella*. White arrow shows bacterial debris in close association with the bead phagosome. Scale bar: 2 µm. **B.** The percentage of beads that was positive for *Legionella* fragments from experiments described in A. Data is represented as mean ± SEM of 3 independent experiments, where 20 cells were quantified for each control/treatment per independent experiment. **C.** Macrophages were presented with mRFP1-*E. coli* (primary target) for 7 h before being challenged with ZsGreen-*E. coli* (secondary target) for the indicated time point. As a control, resting macrophages were

challenged only with the secondary target. Scale bars: main panels = 10 μm; insets = 2 μm. **D.** Quantification of mean mRFP1 fluorescence intensity (derived from primary phagosomes) on ZsGreen-E. coli-containing secondary phagosomes as described in B. Data was normalized to no primary phagocytosis group and presented as mean ± SD of 148-348 cells across 3 independent experiments. Conditions were compared statistically using a one-way ANOVA with Tukey's post-hoc test (**, $p < 0.01$; ***, $p<0.001$).

Figure 10: Clathrin-mediated phagosome resolution is required for degradative capacity of macrophages. A and **C.** Macrophages internalized IgG-opsonized beads (no DQ-BSA) or *E. coli* for 1 or 6 h before the addition of a secondary target, DQ-BSA-opsonized beads. Coverslips were immunostained against external beads (both DQ-BSA labeled and unlabeled beads; green) and imaged live. The lower panels show the red channel (DQ-BSA) in fire scale. Scale bar = 10 μm. For C, macrophages were treated with the clathrin inhibitor, ikarugamycin (IKA), or vehicle (DMSO) 1 h after phagocytosis. **B** and **D.** Quantification of mean DQ-BSA fluorescence intensity of internalized DQ-BSA beads from experiments described in A (B) and C (D). Mean intensity of internal DQ-BSA beads were corrected by subtracting the mean intensity of external DQ-BSA beads. Data is presented as mean ± SEM. For B, data is based on 6 independent experiments, where 150-503 cells were quantified per condition; For D, data is from 27 images across 3 independent experiments, with each image containing 1 to 8 cells. Statistical analysis was done as before. **E.** Ratio of the mean fluorescence intensity of DQ-BSA in ikarugamycin-treated cells to DMSO-treated cells as shown in D. Data is presented as mean ± SEM of 27 images across 3 independent experiments. Statistical analysis was done using an unpaired t-test (*, $p < 0.05$; **, $p< 0.01$; ***, $p<0.001$; ns, not significant).

Supplemental Materials

Supplemental Figure S1: Fragmentation of phagosomes enclosing nanobead clusters. Fluorescent 100 nm latex beads were aggregated using human IgG and presented to RAW macrophages for 2 h before the commencement of live cell imaging. The main panels show the far-red channel in a rainbow scale, where red is the highest intensity level and blue is the lowest intensity level. The smaller panels show the far-red and DIC channels for the first frame of the movie. White dotted lines indicate the boundary of the cell. Scale bar: 10 µm.

Supplemental Figure S2. A. RAW macrophages were presented with mRFP1-*E. coli* for 40 min before treatment with the dynamin inhibitor, dyngo 4a (5 µM), or vehicle (DMSO). The cells were fixed 1 and 4 h post-phagocytosis and immunostained against *E. coli*. Images are displayed as described for A. **B.** The total volume of PDVs for experiments shown in A was quantified per cell. PDVs were quantified as objects if they possessed lower fluorescence intensity than full phagosomes and if their volume was >0.02 μm^3 and <1 μm^3. The volume measurements were normalized to the first measurement (T_0) for the respective treatment. Data are presented as the mean ± SEM of 3 independent experiments and * $p < 0.05$ indicates that the slopes of the regression lines are significantly different.

Supplemental Figure S3: Overview of the quantification method used to determine the total volume of phagosomes and PDVs in each cell. A. A still image from the same video displayed

in Figure 2B is used to exemplify the quantification method. The main panel shows the red channel in a rainbow scale, where red is the highest intensity level and blue is the lowest intensity level. The smaller panels show the red and DIC channels. The white dotted line indicates the boundary of the cell and the white boxes indicate the positions of the insets. Arrows within the insets point to phagosomes, while arrowheads point to PDVs. Scale bars: main panels = 10 μm; insets = 2 μm. **B.** To quantify the total volume of phagosomes in each cell, we drew a region of interest around the cell and instructed Volocity to select objects within that region, which had a high fluorescence intensity and a volume greater than 1 μm^3 (phagosomes are under the masked areas). The volume of phagosomes in each region of interest were summed to determine the total volume of phagosomes in each cell. The volumes of the phagosomes displayed in the insets is indicated. **C.** To quantify the total volume of PDVs in each cell, we instructed Volocity to select dimmer objects within the region of interest enclosing the cell, which had a volume greater than 0.02 μm^3, but less than 5 μm^3 (PDVs are under the masked areas). The volume of PDVs in each region of interest were summed to determine the total volume of PDVs in each cell. Phagosomes were excluded from the PDV quantification, since the inclusion of lower fluorescence intensity PDVs immediately surrounding the phagosomes were included in the phagosomal volume, which increased the apparent size of the phagosomes above the PDV threshold. **D.** To demonstrate that the enlarged phagosomes are excluded from the PDV quantification (in C.), we modified the PDV settings to select the objects that had a volume greater than 5 μm^3. The volumes of these enlarged phagosomes are indicated for comparison with phagosomes quantified in B.

Supplemental Video 1. Bead-containing phagosomes remain within macrophages over 24 h. RAW macrophages were allowed to internalize IgG-opsonized latex beads for 2 h before cells were moved to a pre-warmed (37°C) microscope stage. Images were acquired at a rate of 1 frame/h for a 24-hour period. Still frames from Video 1 are displayed in Figure 1A. Scale bar: 10 µm.

Supplemental Video 2. Ionomycin treatment does not trigger exocytosis of bead-containing phagosomes. IgG-opsonized latex beads were presented to RAW cells for 1 h before cells were moved to a pre-warmed (37°C) microscope stage. After acclimatization, the cells were exposed to media containing 10 µM of ionomycin and 1.2 mM of Ca^{2+} and imaging commenced immediately. Images were acquired at a rate of 12 frames/h for a 1-hour period. Still frames from Video 2 are displayed in Figure 1C. Scale bar: 2 µm.

Supplemental Video 3. Phagosomes containing mCherry-*Legionella* undergo fragmentation. RAW macrophages were challenged with IgG-opsonized, filamentous mCherry-*Legionella* for 7 h before the cells were moved to a pre-warmed (37°C) microscope stage. Images were acquired at a rate of 6 frames/h for a 13-hour period. The mCherry fluorescence intensity is displayed as a rainbow scale, where red is the highest intensity level and blue is the lowest intensity level. Still frames from Video 3 are displayed in Figure 2A. Scale bar: 2 µm.

Supplemental Video 4. Fission of phagosomes containing ZsGreen-*E. coli*. Macrophages were allowed to internalize ZsGreen-*E. coli* and imaging was started immediately. Images were

acquired at a rate of 2 frames/h for a 10-hour period. Scale bar = 10 µm. Video 4 is complementary to Figure 2C. Scale bar: 2 µm.

Supplemental Video 5. Budding of phagosomes containing intact mRFP1-*E. coli*. Macrophages were allowed to internalize mRFP1-*E. coli* and imaging was started 15 min after phagocytosis. mRFP1-positive vesicles presented as pseudocolour to enhance visibility of low-intensity events. Images were acquired at 1 frame every 3 seconds. Scale bar = 2 µm.

Supplemental Video 6. Budding of phagosomes containing degraded mRFP1-*E. coli*. Macrophages were allowed to internalize mRFP1-*E. coli* and imaging was started 180 minutes after phagocytosis. mRFP1-positive vesicles presented as pseudocolour to enhance visibility of low-intensity events. Images were acquired at 1 frame every 3 seconds. Scale bar = 2 µm.

Supplemental Video 7. Tubulation of phagosomes containing mRFP1-*E. coli*. Macrophages were allowed to internalize mRFP1-*E. coli* and imaging was started 180 minutes after phagocytosis. mRFP1-positive vesicles presented as pseudocolour to enhance visibility of low-intensity events. Images were acquired at 1 frame every 3 seconds. Scale bar = 2 µm.

Supplemental Video 8. Splitting of phagosomes containing mRFP1-*E. coli*. Macrophages were allowed to internalize mRFP1-*E. coli* and imaging was started 150 minutes after phagocytosis. mRFP1-positive vesicles presented as pseudocolour to enhance visibility of low-intensity events. Images were acquired at 1 frame every 3 seconds. Scale bar = 2 µm.

Supplemental Video 9. Phagosomes containing fluorescent bead clumps undergo fragmentation. Cy5-labelled 0.1 µm beads were clumped using human IgG and were presented to RAW macrophages for 2 h before the cells were moved to a pre-warmed (37°C) microscope stage. Images were acquired at a rate of 3 frames/h for a 6-hour period. The Cy5 fluorescence intensity is illustrated as a rainbow scale where red is the highest intensity level and blue is the lowest intensity level. Still frames from Video 9 are displayed in Supplemental Figure S1. Scale bar: 2 µm.

Supplemental Video 10. Inhibition of clathrin using pitstop prevents the fragmentation of phagolysosomes containing mCherry-*Legionella*. RAW macrophages were allowed to internalize IgG-opsonized, filamentous mCherry-*Legionella* for 4 h before cells were moved to a pre-warmed (37°C) microscope stage. After acclimatization, the cells were exposed to media containing vehicle control (DMSO) or 10 µM of pitstop 2 and imaging started 10 min after treatment. Images were acquired at a rate of 12 frames/h for a 9.5-hour period. The mCherry fluorescence intensity is illustrated in rainbow scale, where red is the highest intensity level and blue is the lowest intensity level. Still frames from Video 10 are displayed in Figure 6A. Scale bar: 2 µm.

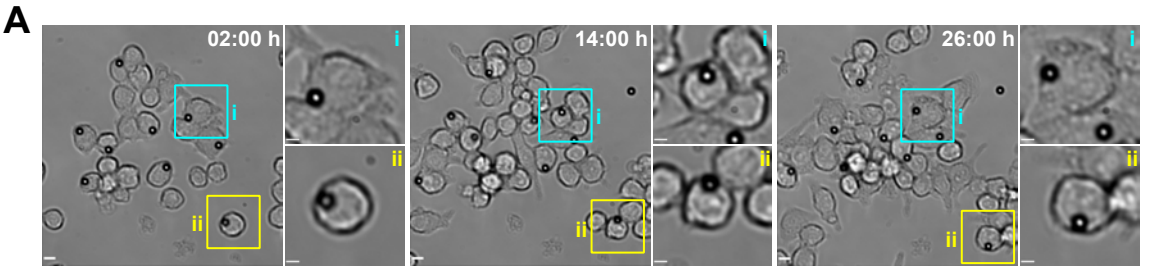
A
02:00 h
14:00 h
26:00 h
i
ii

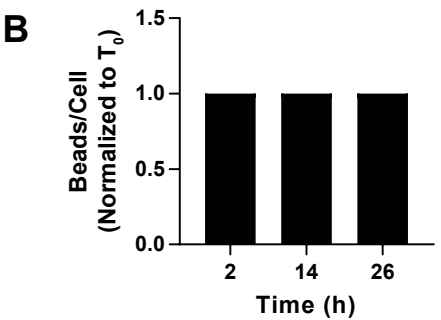
B
Beads/Cell
(Normalized to T0)
1.5
1.0
0.5
0.0
2
14
26
Time (h)

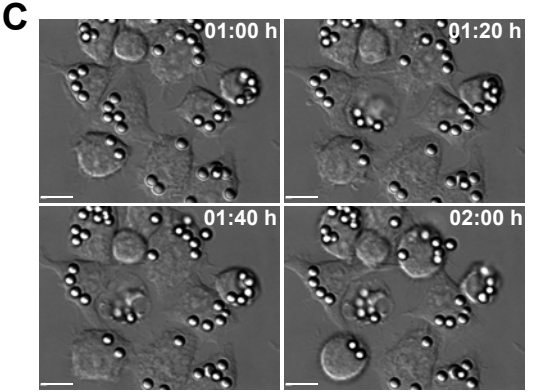
C
01:00 h
01:20 h
01:40 h
02:00 h

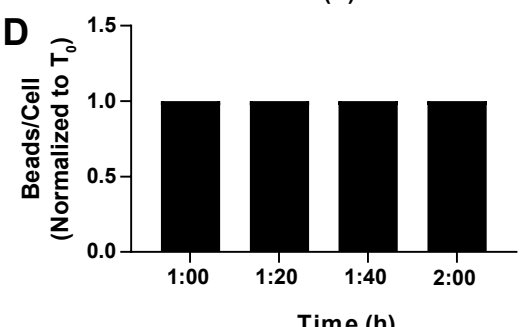
D
Beads/Cell
(Normalized to T0)
1.5
1.0
0.5
0.0
1:00
1:20
1:40
2:00
Time (h)

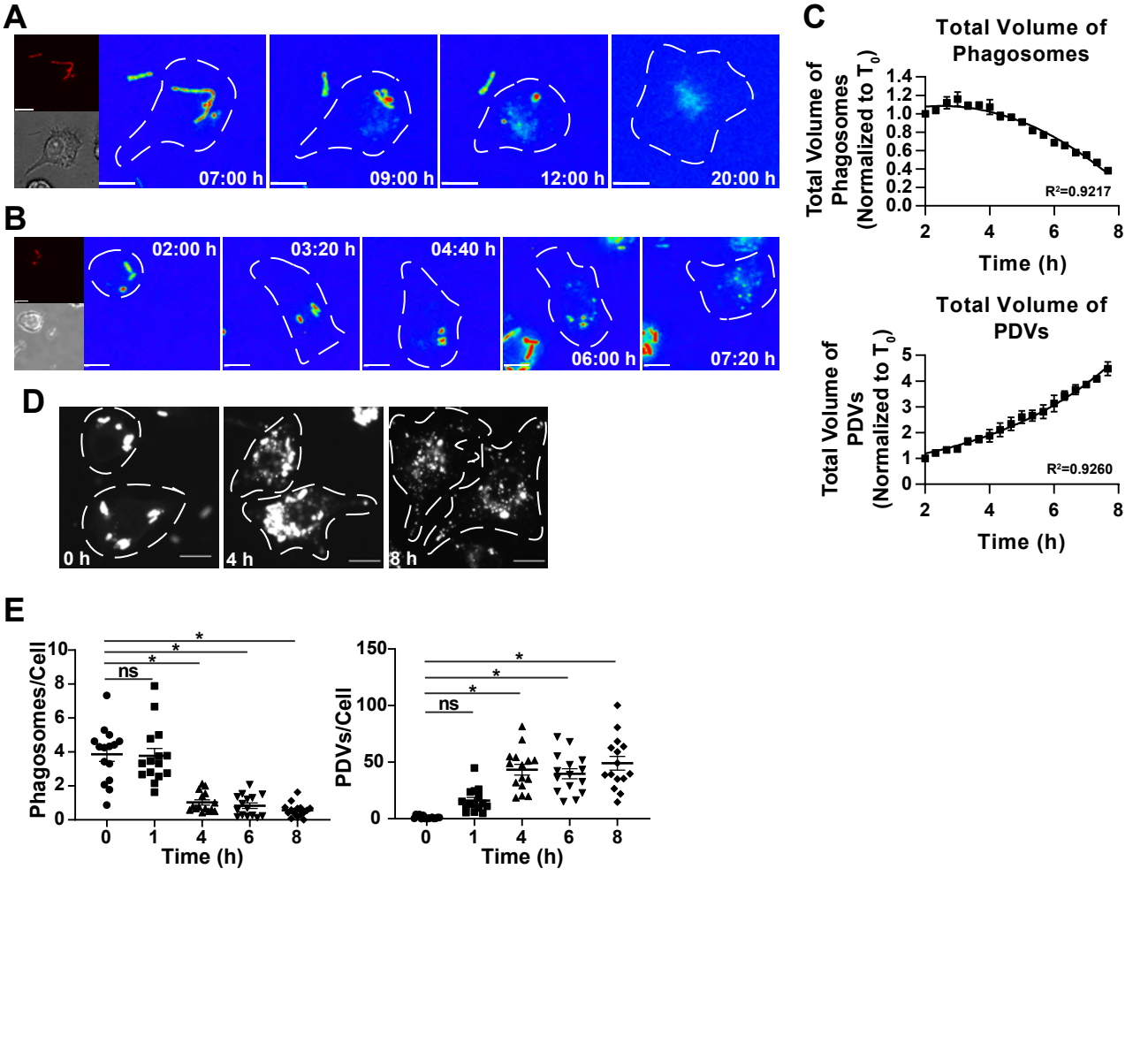
A
07:00 h
09:00 h
12:00 h
20:00 h
B
02:00 h
03:20 h
04:40 h
06:00 h
07:20 h
C
Total Volume of Phagosomes
Total Volume of Phagosomes (Normalized to T0)
R²=0.9217
Time (h)
Total Volume of PDVs
Total Volume of PDVs (Normalized to T0)
R²=0.9260
Time (h)
D
0 h
4 h
8 h
E
Phagosomes/Cell
ns
Time (h)
PDVs/Cell
ns
Time (h)

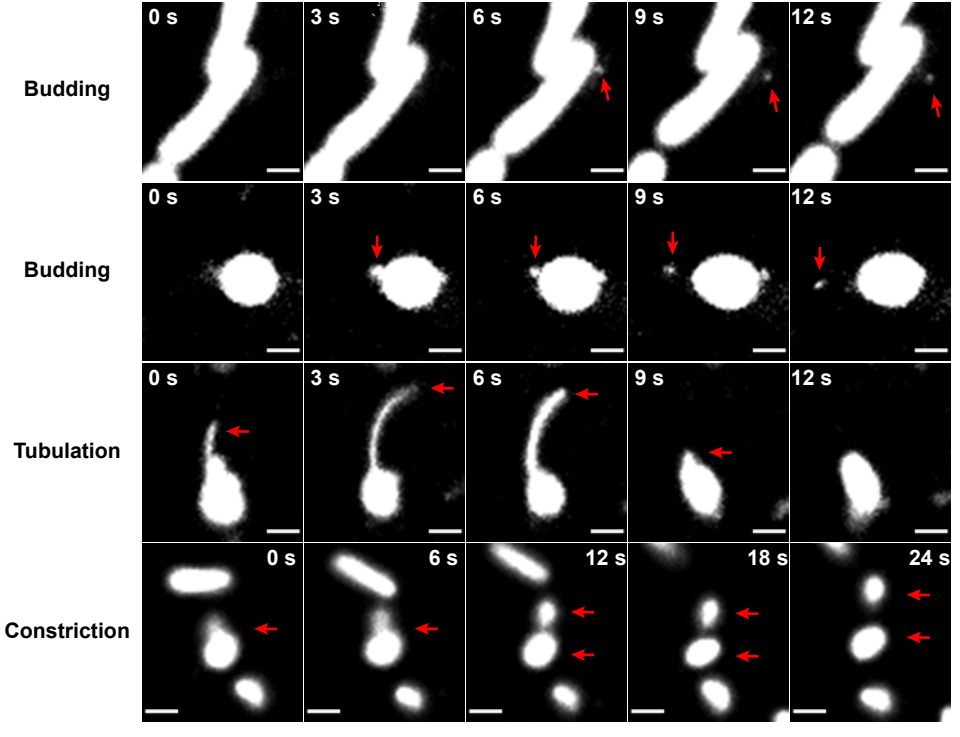
Budding
0 s
3 s
6 s
9 s
12 s
Budding
0 s
3 s
6 s
9 s
12 s
Tubulation
0 s
3 s
6 s
9 s
12 s
Constriction
0 s
6 s
12 s
18 s
24 s

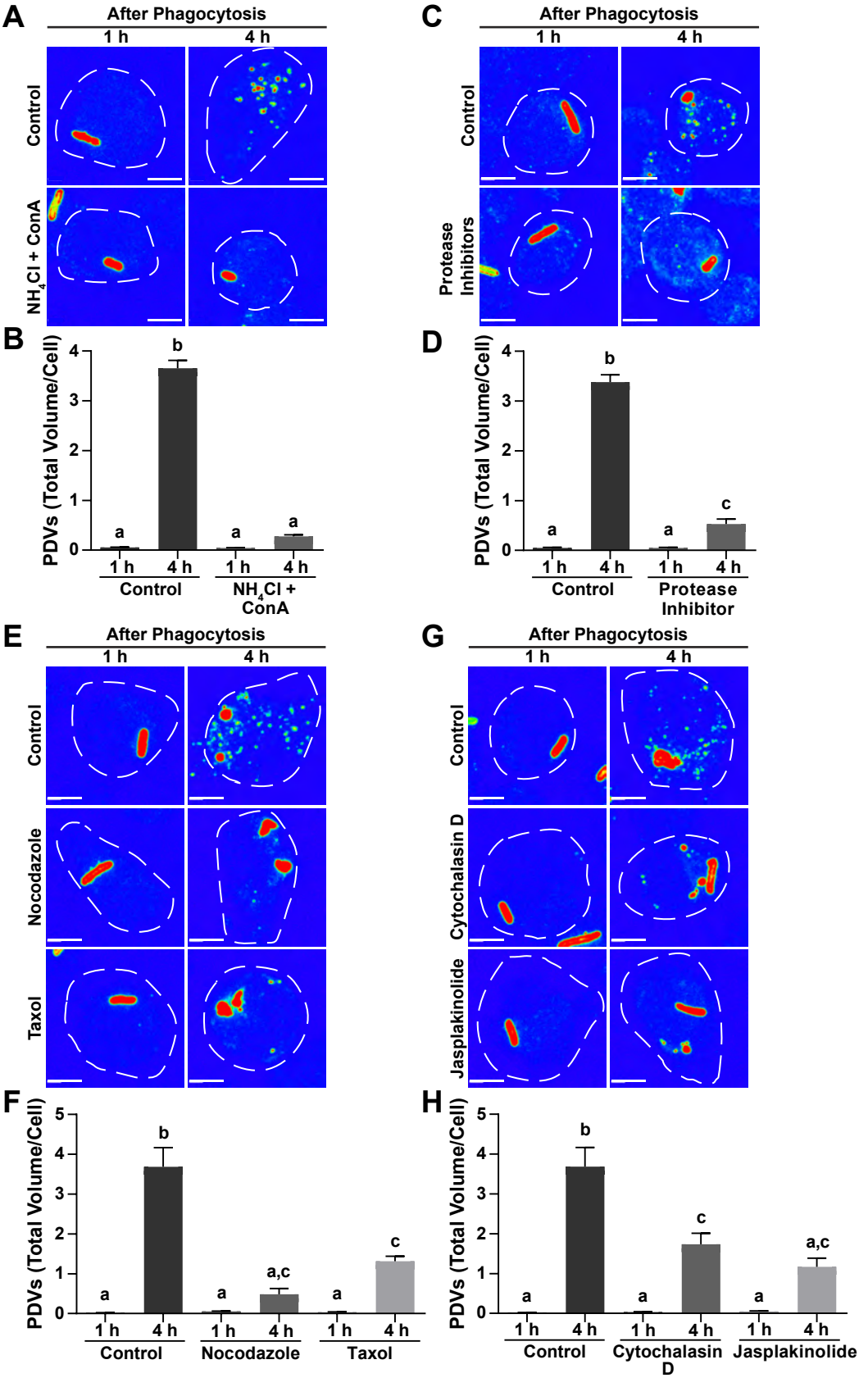
A
After Phagocytosis
1 h
4 h
Control
NH4Cl + ConA
B
PDVs (Total Volume/Cell)
a
b
a
a
1 h
4 h
1 h
4 h
Control
NH4Cl + ConA
C
After Phagocytosis
1 h
4 h
Control
Protease Inhibitors
D
PDVs (Total Volume/Cell)
a
b
a
c
1 h
4 h
1 h
4 h
Control
Protease Inhibitor
E
After Phagocytosis
1 h
4 h
Control
Nocodazole
Taxol
F
PDVs (Total Volume/Cell)
a
b
a
a,c
a
c
1 h
4 h
1 h
4 h
1 h
4 h
Control
Nocodazole
Taxol
G
After Phagocytosis
1 h
4 h
Control
Cytochalasin D
Jasplakinolide
H
PDVs (Total Volume/Cell)
a
b
a
c
a
a,c
1 h
4 h
1 h
4 h
1 h
4 h
Control
Cytochalasin D
Jasplakinolide

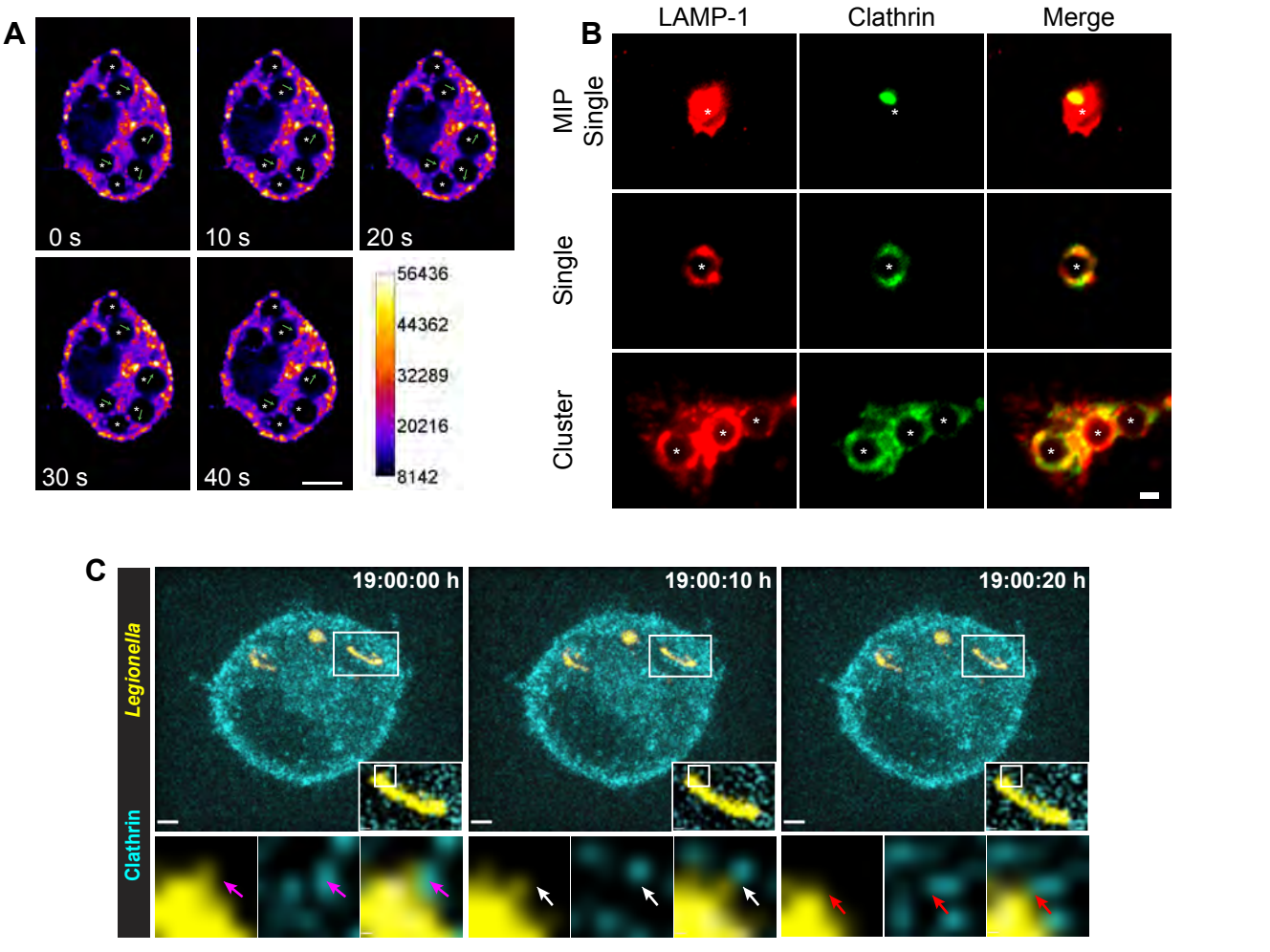
A
0 s
10 s
20 s
30 s
40 s
56436
44362
32289
20216
8142
B
LAMP-1
Clathrin
Merge
MIP
Single
Single
Cluster
C
Legionella
Clathrin
19:00:00 h
19:00:10 h
19:00:20 h

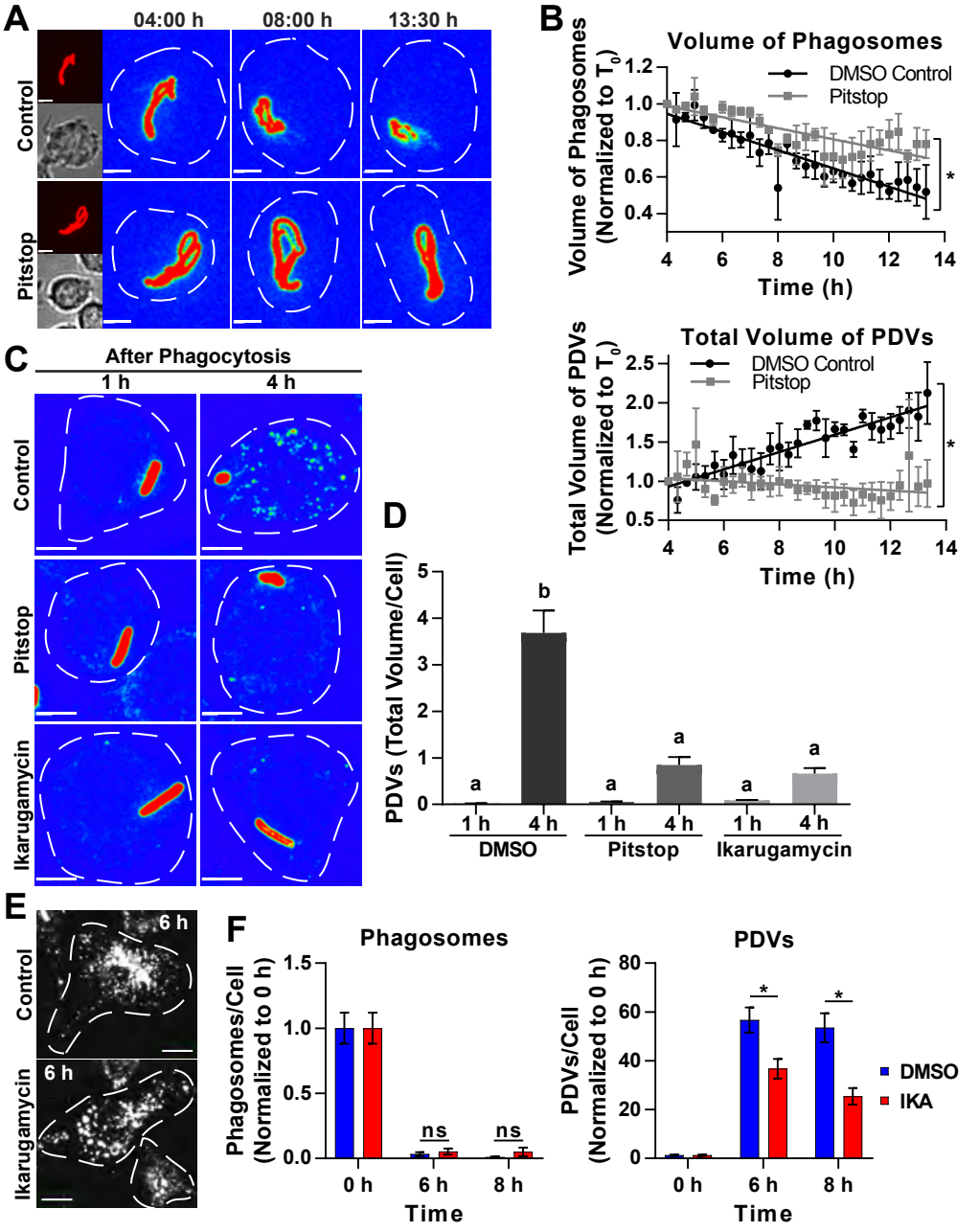
A
04:00 h
08:00 h
13:30 h
Control
Pitstop
B
Volume of Phagosomes
DMSO Control
Pitstop
Volume of Phagosomes (Normalized to T0)
Time (h)
Total Volume of PDVs
Total Volume of PDVs (Normalized to T0)
C
After Phagocytosis
1 h
4 h
Ikarugamycin
D
PDVs (Total Volume/Cell)
DMSO
Pitstop
Ikarugamycin
E
6 h
F
Phagosomes
PDVs
Phagosomes/Cell (Normalized to 0 h)
PDVs/Cell (Normalized to 0 h)
ns
DMSO
IKA
Time

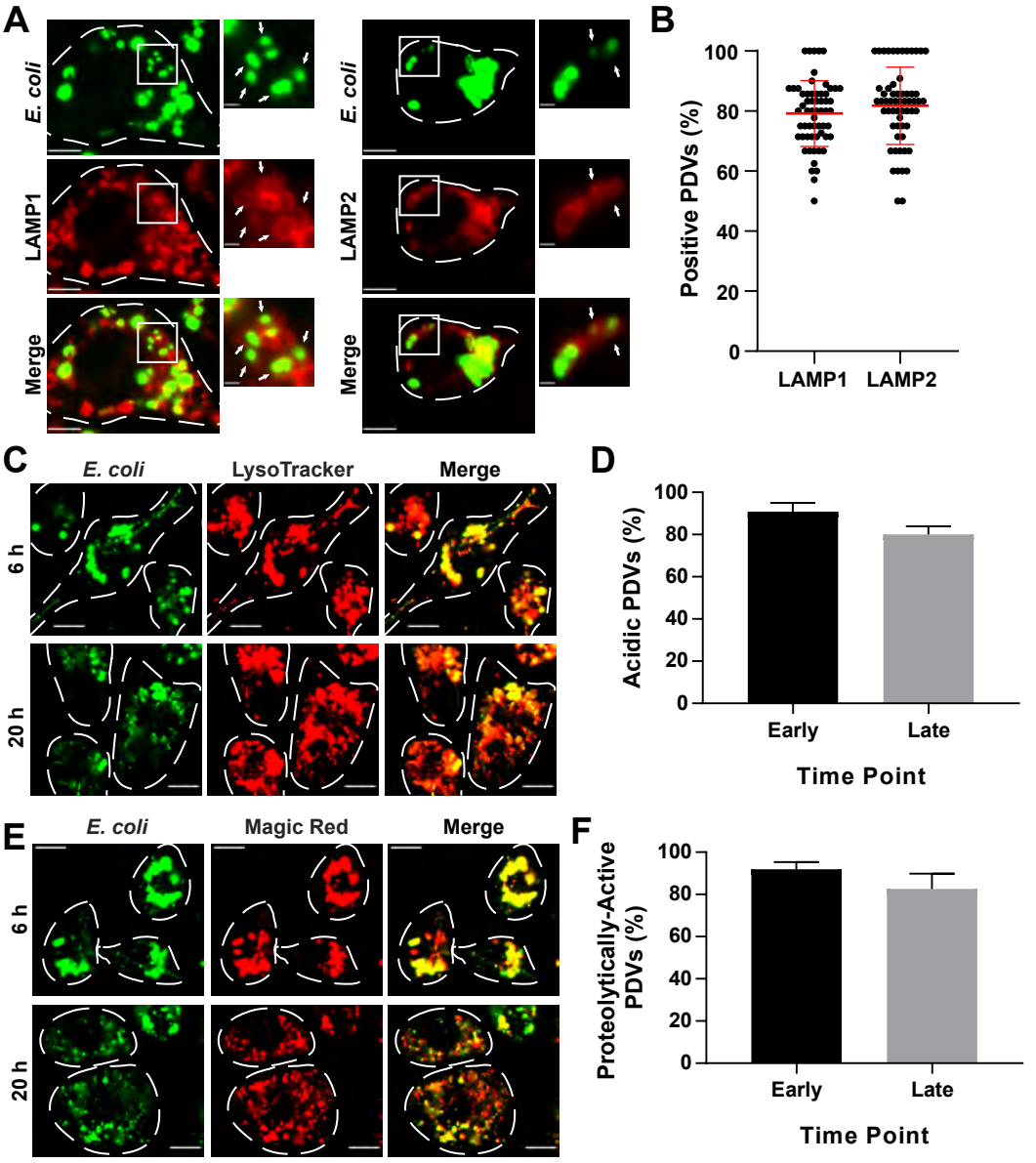
A
E. coli
LAMP1
Merge
E. coli
LAMP2
Merge
B
Positive PDVs (%)
100
80
60
40
20
0
LAMP1
LAMP2
C
E. coli
LysoTracker
Merge
6 h
20 h
D
Acidic PDVs (%)
100
80
60
40
20
0
Early
Late
Time Point
E
E. coli
Magic Red
Merge
6 h
20 h
F
Proteolytically-Active PDVs (%)
100
80
60
40
20
0
Early
Late
Time Point

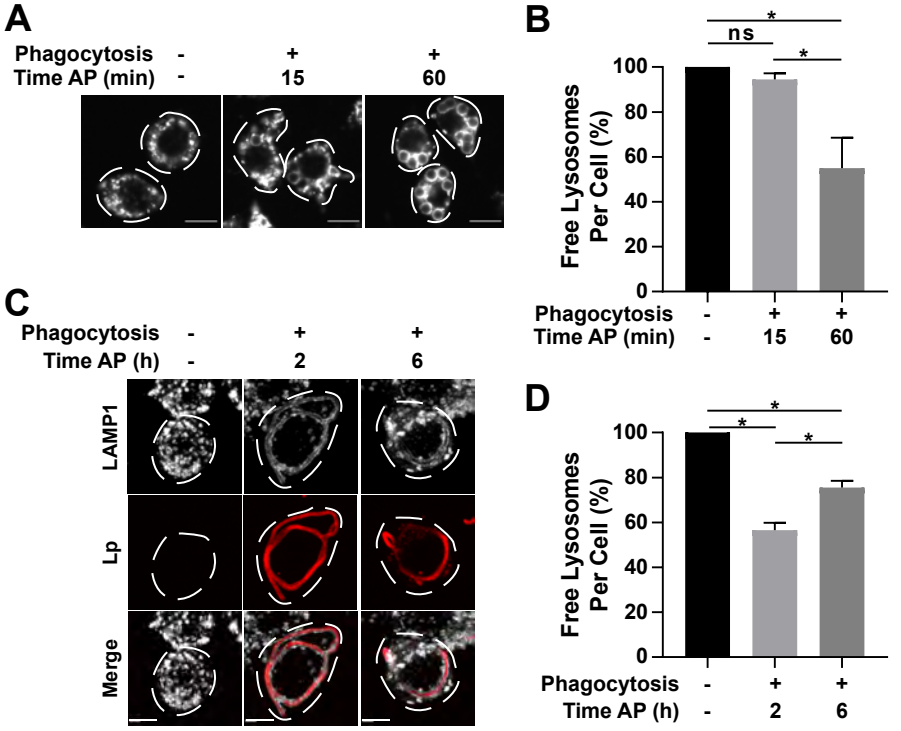
A
Phagocytosis - + +
Time AP (min) - 15 60
B
ns
*
*
Free Lysosomes Per Cell (%)
100
80
60
40
20
0
Phagocytosis - + +
Time AP (min) - 15 60
C
Phagocytosis - + +
Time AP (h) - 2 6
LAMP1
Lp
Merge
D
*
*
*
Free Lysosomes Per Cell (%)
100
80
60
40
20
0
Phagocytosis - + +
Time AP (h) - 2 6

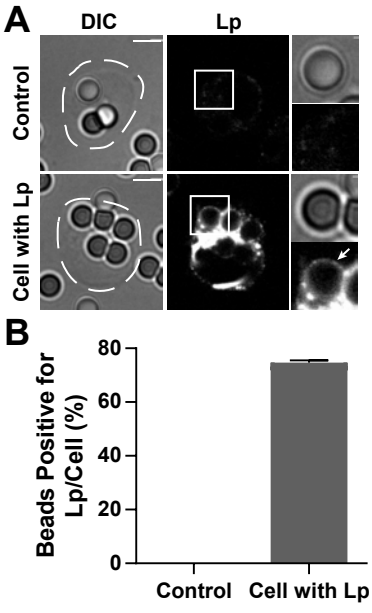
A
DIC
Lp
Control
Cell with Lp
B
Beads Positive for Lp/Cell (%)
80
60
40
20
0
Control
Cell with Lp
C
Primary Target - +
Secondary Target + +
Time AP (h; 2nd Target) 0 0
Primary Target
Secondary Target
1309
1000
690
381
72
D
Normalized Primary Target Fluorescence
15
10
5
0
-5
**
***
Primary Target - + +
Secondary Target + + +
Time AP (h; 2nd Target) 0 0 2

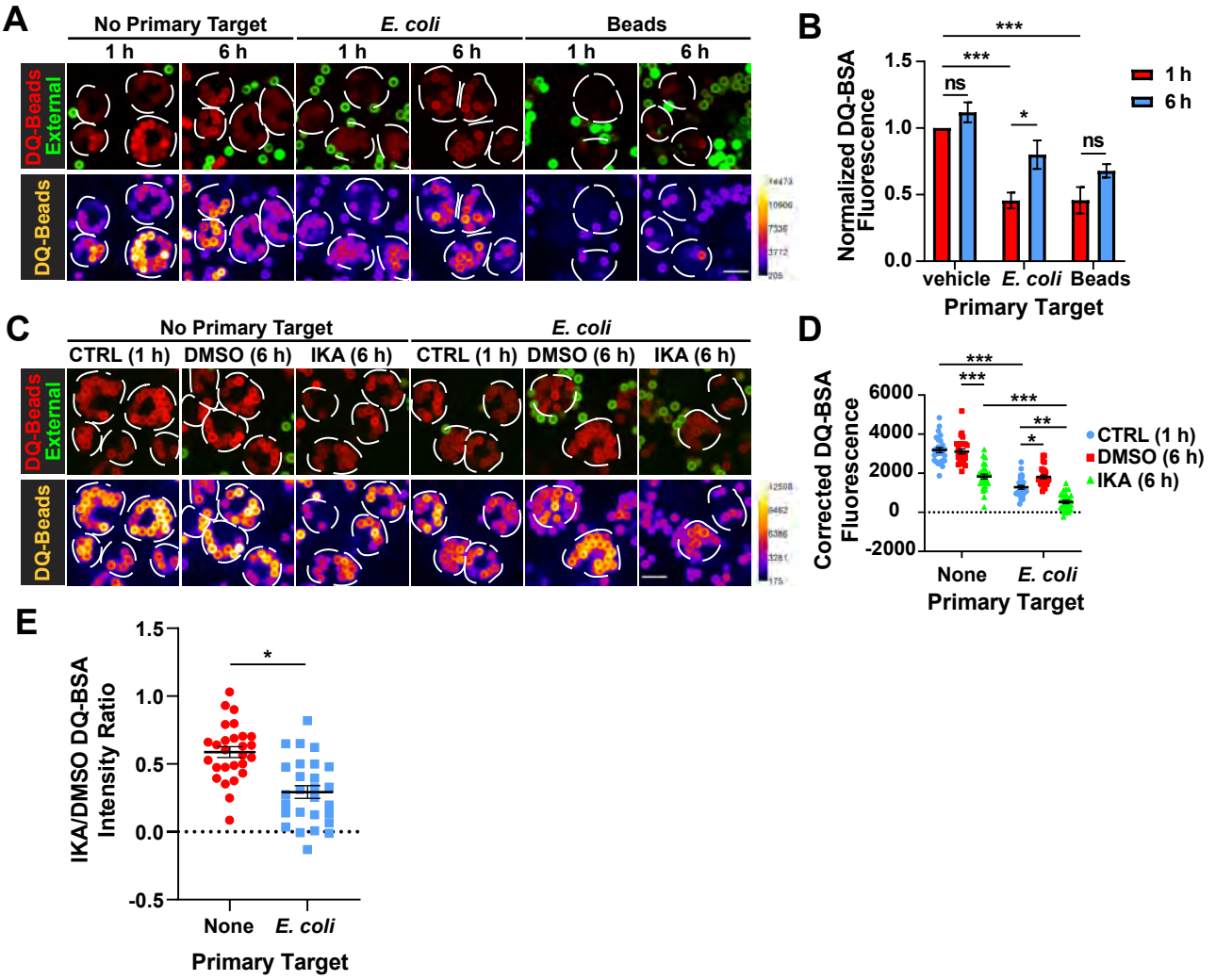
A
No Primary Target
E. coli
Beads
1 h
6 h
1 h
6 h
1 h
6 h
DQ-Beads External
DQ-Beads
B
Normalized DQ-BSA Fluorescence
1.5
1.0
0.5
0.0
***
***
ns
*
ns
1 h
6 h
vehicle
E. coli
Beads
Primary Target
C
No Primary Target
E. coli
CTRL (1 h)
DMSO (6 h)
IKA (6 h)
CTRL (1 h)
DMSO (6 h)
IKA (6 h)
DQ-Beads External
DQ-Beads
D
Corrected DQ-BSA Fluorescence
6000
4000
2000
0
-2000
***
***
***
**
*
CTRL (1 h)
DMSO (6 h)
IKA (6 h)
None
E. coli
Primary Target
E
IKA/DMSO DQ-BSA Intensity Ratio
1.5
1.0
0.5
0.0
-0.5
*
None
E. coli
Primary Target